

Cover Page



Universiteit Leiden



The handle <http://hdl.handle.net/1887/43389> holds various files of this Leiden University dissertation

Author: Bingen, Brian O.

Title: Molecular and cellular determinants of cardiac tachyarrhythmias: from trigger to therapy

Issue Date: 2016-10-05

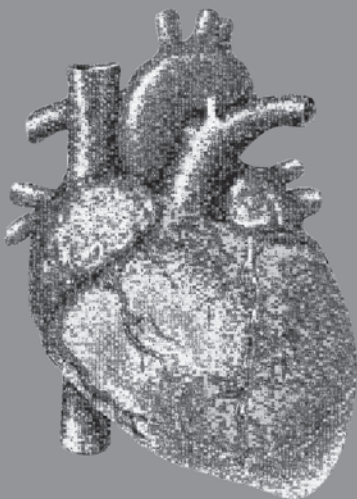
Chapter IV

Atrium-specific Kir3.x determines inducibility, dynamics and termination of fibrillation by regulating restitution-driven alternans.

Kir3.x in Atrial Fibrillation

Brian O. Bingen, MD; Zeinab Neshati, MSc; Saïd F. A. Askar, MSc; Ivan V. Kazbanov, MSc; Dirk L. Ypey, PhD; Alexander V. Panfilov, PhD; Martin J. Schaliq, MD, PhD; Antoine A. F. de Vries, PhD; Daniël A. Pijnappels, PhD.

Circulation. 2013;128:2732-44.



ABSTRACT

Background: Atrial fibrillation (AF) is the most common cardiac arrhythmia. Ventricular pro-arrhythmia hinders pharmacological AF treatment. Modulation of atrium-specific Kir3.x channels, which generate a constitutively active current ($I_{K_{ACh-c}}$) after atrial remodeling, might circumvent this problem. However, it is unknown whether and how $I_{K_{ACh-c}}$ contributes to AF induction, dynamics and termination. Therefore we investigated the effects of $I_{K_{ACh-c}}$ blockade and Kir3.x downregulation on AF.

Methods and Results: Neonatal rat atrial cardiomyocyte cultures and intact atria were burst paced to induce reentry. To study the effects of Kir3.x on action potential characteristics and propagation patterns, cultures were treated with tertiapin or transduced with lentiviral vectors encoding *Kcnj3*- or *Kcnj5*-specific short hairpin RNAs. Kir3.1 and Kir3.4 were expressed in atrial but not in ventricular cardiomyocyte cultures. Tertiapin prolonged action potential duration (APD; 54.7 ± 24.0 to 128.8 ± 16.9 ms, $p < 0.0001$) in atrial cultures during reentry, indicating the presence of $I_{K_{ACh-c}}$. Furthermore, tertiapin decreased rotor frequency (14.4 ± 7.4 to 6.6 ± 2.0 Hz, $p < 0.05$) and complexity (6.6 ± 7.7 to 0.6 ± 0.8 phase singularities, $p < 0.0001$). Knockdown of *Kcnj3* or *Kcnj5* gave similar results. Blockade of $I_{K_{ACh-c}}$ prevented/terminated reentry by prolonging APD and changing APD and conduction velocity (CV) restitution slopes, thereby altering the probability of APD alternans and rotor destabilization. Whole heart mapping experiments confirmed key findings (e.g. $>50\%$ reduction in AF inducibility after $I_{K_{ACh-c}}$ blockade).

Conclusions: Atrium-specific Kir3.x controls induction, dynamics and termination of fibrillation by modulating APD and APD/CV restitution slopes in atrial tissue with $I_{K_{ACh-c}}$. This study provides new molecular and mechanistic insights into atrial tachyarrhythmias and identifies Kir3.x as a promising atrium-specific target for antiarrhythmic strategies.

INTRODUCTION

Atrial fibrillation (AF) is the most common cardiac rhythm disorder in humans, and substantially contributes to morbidity, mortality and health care costs.¹⁻³ Ablation techniques, breaking up AF circuits or triggers, have improved the outcome of AF in the past decades.⁴ While the success rate of AF ablation is relatively high in paroxysmal AF, in permanent AF ablation restores sinus rhythm only in a fraction of patients, due to altering underlying mechanisms and structural changes of the atrial myocardium. Importantly, there is a lack of consensus on the optimal ablation strategy in these patients, while this population is vastly growing.^{5,6} In addition, ablation procedures are associated with a risk of complications due to their invasive nature.⁷ Furthermore, long-term maintenance of sinus rhythm requires repeated procedures or continuation of anti-arrhythmic drugs in a significant proportion of chronic AF patients.⁸ Hence, first line treatment of AF is still performed pharmacologically.⁴ However, the use of anti-arrhythmic agents is hampered by potentially lethal ventricular pro-arrhythmia, lack of efficacy and serious side effects.⁹⁻¹³ Thus, research on AF treatment has focused on finding atrium-selective drugs, with higher efficacy in AF rhythm control but less side effects such as ventricular pro-arrhythmia.

In the heart of most mammals, including humans, the acetylcholine-activated potassium current ($I_{K,ACh}$) is found exclusively in the atrium.¹⁴ Hence, $I_{K,ACh}$ is one of the novel candidates for atrium-specific drug treatment. Activating $I_{K,ACh}$ by acetylcholine has been shown to shorten action potential (AP) duration (APD) in the atria.¹⁵ In patients suffering from persistent AF and atrial remodeling, $I_{K,ACh}$ can become constitutively active.^{16,17} Whether this constitutively active acetylcholine-inducible current ($I_{K,ACh-c}$) affects AF induction, dynamics or termination, the mechanisms by which it could do so, as well as the channels involved in this process remain to be elucidated.

To test whether and how $I_{K,ACh-c}$ affects fibrillation, a 2D *in vitro* model of atrial tissue and a whole heart model of AF were developed using atrial neonatal rat cardiomyocytes (nrCMCs) and hearts with endogenous $I_{K,ACh-c}$. Using these models, fibrillation could be systematically and reproducibly studied. Inhibition of Kir3.1 or Kir3.4 activity by the highly specific drug tertiapin or lentiviral vector (LV)-mediated RNA interference (RNAi), was used to study the role of $I_{K,ACh-c}$ in AF initiation, dynamics and termination.

METHODS

A detailed description of materials and methods can be found in the Supplementary Material online.

All animal experiments were approved by the Animal Experiments Committee of the Leiden University Medical Center and conformed to the Guide for the Care and Use of Laboratory Animals as stated by the US National Institutes of Health.

Cell isolation and culture

After careful separation of the atria and ventricles of neonatal Wistar rat hearts, cardiomyocytes were isolated by collagenase digestion and plated on fibronectin-coated, round glass coverslips (15-mm diameter) at a density of $2-8 \times 10^5$ cells/well in 24-well cell culture plates, as described previously.¹⁸ To restrict unwanted expansion of the remaining non-myocytes, cell proliferation was inhibited by incubation with Mitomycin-C (10 µg/ml; Sigma-Aldrich, St. Louis, MO) for 2 h at day 1 of culture.¹⁹

Western blotting

Cardiomyocytes were lysed in 50 mM Tris-HCl (pH 8.0), 150 mM NaCl, 1% Triton X-100, 0.5% sodium deoxycholate, 0.1% sodium dodecyl sulfate. Three 15-mm wells, each seeded with 8×10^5 cells, were used for each sample, and each experiment consisted of at least 4 samples. The proteins in the lysate were size-fractionated in NuPage Novex 12% Bis-Tris gels (Life Technologies, Bleiswijk, the Netherlands) and transferred to Hybond polyvinylidene difluoride membranes (GE Healthcare, Diegem, Belgium). Membranes were blocked in Tris-based saline, 0.1% Tween-20, 5% bovine serum albumin (Sigma-Aldrich) for 1 h. Next, membranes were incubated with antibodies directed against Kir3.1 (Alomone Labs, Jerusalem, Israel), Kir3.4 (Santa Cruz Biotechnology, Dallas, TX) or glyceraldehyde 3-phosphate dehydrogenase (GAPDH; loading control; Merck Millipore, Billerica, MA) and corresponding horseradish peroxidase-conjugated secondary antibodies (Santa Cruz Biotechnology) for 1 h. Chemiluminescence was detected using ECL Prime Western blot detection reagent (GE Healthcare).-

Optical mapping

At day 9 of culture, investigation of AP propagation on a whole-culture scale by optical mapping (using di-4-ANEPPS [Life Technologies] as voltage-sensitive dye) and subsequent data analyses were performed as described previously.¹⁸ During optical mapping cells were stimulated electrically using a custom-made, epoxy-coated unipolar platinum electrode with square suprathreshold electrical stimuli at 1 and 2-20 Hz (2-Hz increments). Burst pacing with a cycle length of 20-100 ms was used to induce reentry. Complexity was defined as the number of phase singularities (PSs) per cm^2 , determined by using the phase space method as described previously.¹⁸ The effect of several drugs (100 nmol/L tertiapin [Alomone Labs], 200 nmol/L atropine [Sigma-Aldrich] and 2 µmol/L carbachol [Sigma-Aldrich])¹⁶ was studied by pipetting them directly into the medium, dispersing them by gentle agitation, immediately followed by optical mapping.

Whole heart mapping was performed by incubating neonatal rat hearts with 2 μM di-4-ANEPPS in a tissue bath containing oxygenated Tyrode's solution (comprising [in mM] NaCl 130, CaCl_2 1.8, KCl 4.0, MgCl_2 1.0, NaH_2PO_4 1.2, NaHCO_3 24 and glucose 5.5 at pH 7.4). Prior to excision of the heart, the left ventricle was injected with Tyrode's solution supplemented with 20 mM 2,3-butanedione monoxime (Sigma-Aldrich) to minimize motion artifacts with or without 200 nM tertiapin to block Kir3.x channels. During whole heart mapping, AF was induced by burst pacing at a cycle length of 20-100 ms using a custom-made bipolar platinum electrode.

RNAi

Kir3.1 and Kir3.4 expression in neonatal rat atrial cell cultures was selectively inhibited using self-inactivating LVs encoding short hairpin (sh) RNAs specific for rat *Kcnj3* (LV-Kir3.1 \downarrow) and *Kcnj5* (LV-Kir3.4 \downarrow), respectively. The shuttle constructs to generate these LVs are derivatives of plasmid SHC007 from the Mission shRNA library (Sigma-Adrich) in which the *Photinus pyralis luciferase (PpLuc)*-specific shRNA-coding sequence was replaced by a rat *Kcnj3*- or *Kcnj5*-specific shRNA-coding sequence and the marker gene cassette consisting of the human *phosphoglycerate kinase 1* gene promoter and the puromycin-N-acetyltransferase-coding sequence was substituted by the human *eukaryotic translation elongation factor 1 alpha 1* gene promoter and the *Aequorea victoria* enhanced green fluorescent protein-coding sequence. The negative control vector (LV-PpLuc \downarrow) had the same genetic makeup, except that it contained the aforementioned *PpLuc*-specific shRNA-coding sequence.

Statistical analysis

Statistical analyses were performed using SPSS11.0 for Windows (SPSS, Chicago, IL). Comparison between two groups was performed using the Mann-Whitney U test or Wilcoxon signed rank test or Fisher's exact test where appropriate. Kruskal-Wallis testing with Bonferoni *post-hoc* correction was used for multiple groups and comparisons. Data were expressed as mean \pm standard deviation (SD) for a number (n) of observations. Differences were considered statistically significant if $p < 0.05$. Non-linear regression curves were constructed by using a robust exponential one-phase decay curve fit. Accuracy of these curves was expressed as the coefficient of determination (R^2). R^2 was calculated by the formula $R^2 = 1 - (SS_{\text{reg}}/SS_{\text{tot}})$ where SS_{reg} is the regression sum of squares (the sum of the square vertical distances of individual points to the regression curve) and SS_{tot} is the total sum of squares (the sum of the square vertical distances to the mean of all Y values).

RESULTS

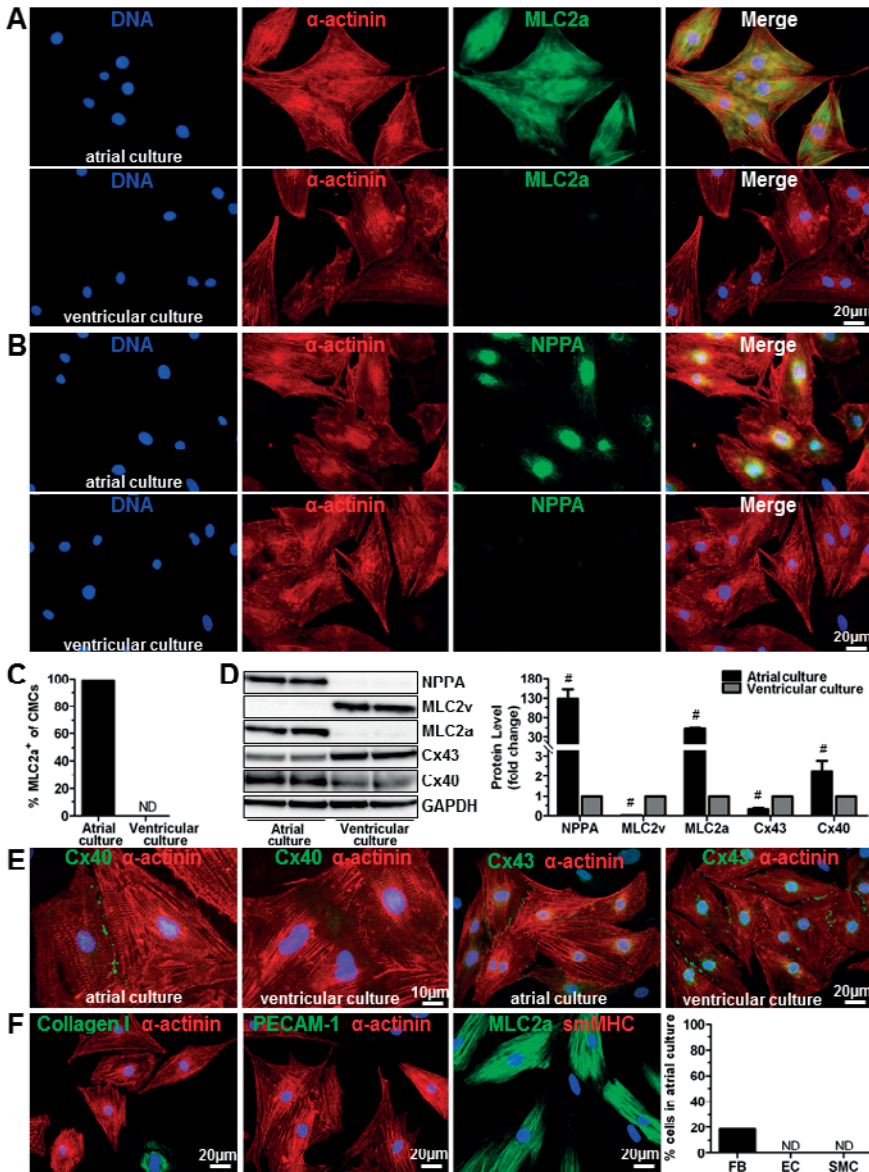
Cell culture characteristics

A detailed characterization of atrial and ventricular nrCMC cultures by immunocytology and Western blotting can be found in the Supplementary Material online (Supplemental Figure 1).

Activation pattern characteristics in atrial nrCMC cultures

During optical mapping, atrial cultures showed uniform, convex and fast activation originating from the electrode upon 1-Hz stimulation (Figure 1A). After burst pacing, reentry was induced in the vast majority of atrial cultures. In 46 out of 49 of these arrhythmic cultures activation patterns remained stable during each cycle of reentry, while also the number and spatial dispersion of PSs did not change during 6 s of mapping (Figure 1B, Supplemental Movie 1). Return mapping (plotting a peak-to-peak interval [PPI] against the subsequent PPI) and time series of the PPIs showed that through such a fixed activation pattern and PS position these arrhythmias had period-1 (P-1) oscillatory dynamics (*i.e.* all rotor periods had approximately the same length) (Supplemental Figure 2A,C,E). Interestingly, the remaining 6% of cultures showed changes in activation pattern, PS number and PS position for each reentrant cycle (Figure 1C, Supplemental Movie 2). Return mapping and time series of the PPIs in these cultures showed period>1 or aperiodical oscillatory dynamics (*i.e.* the wavefront rotation alternated between >1 different periods or showed a different period during each cycle) (Supplemental Figure 2B,D,F).

During burst pacing-induced reentry (including both the stable and the unstable cases of reentry, $n=49$), rotor frequency showed a hyperbolic-like relationship with both APD_{80} ($R^2=0.91$) and wavelength ($R^2=0.63$). No apparent relation was found between rotor frequency and conduction velocity (CV) (Figure 1D-F). Moreover, the number of rotors negatively correlated with wavelength ($R^2=0.73$) and APD_{80} ($R^2=0.70$). Again CV, other than its effects on wavelength did not show a strong individual correlation with the number of PSs during reentry (Figure 1G-I). These results show that fibrillatory activation in this model can be maintained by P-1 or period>1/aperiodical reentry. Furthermore, the correlation analyses suggest that prolongation of atrial APD and wavelength during AF could decrease rotor frequency as well as complexity, possibly leading to prevention or termination of AF.



Supplemental Figure I. Typical examples of immunocytological double staining of (A) MLC2a (green) and α -actinin (red) and (B) NPPA (green) and α -actinin (red) in atrial (upper panels) and ventricular (lower panels) neonatal rat CMC cultures. (C) Quantification of MLC2a and α -actinin double-positive cells in atrial and ventricular neonatal rat CMC cultures. (D) Western blot analysis (left) and quantification (right) of NPPA, MLC2v, MLC2a, Cx43 and Cx40 levels in atrial and ventricular neonatal rat CMC cultures using GAPDH as loading control. (E) Immunocytological double staining of Cx40 (green) and α -actinin (red) and of Cx43 (green) and α -actinin (red) in atrial (1st and 3rd panel from the left, respectively) and ventricular (2nd and 4th panel from the left, respectively) neonatal rat CMC cultures. (F) Immunocytological double staining of collagen type I (green, left) and PECAM-1 (green, middle) with α -actinin (red) and of MLC2a (green, right) with smMHC (red, right). The corresponding quantification of fibroblasts (FB), endothelial cells (EC) and smooth muscle cells (SMC) is depicted on the far right. #: $p < 0.05$ vs ventricular cultures, ND: not detected.

Blockade of atrium-specific $I_{K,ACh}$ decreases rotor frequency, complexity and inducibility of reentry

Atrial nrCMCs abundantly expressed Kir3.1 and Kir3.4 in comparison to ventricular nrCMCs (100.0 ± 6.3 vs 18.3 ± 0.7 and 100 ± 2.8 vs $7.8 \pm 2.0\%$, respectively, $p < 0.05$, $n = 4$ per group) as judged by Western blot analyses (Figure 2A). As such, Kir3.x could be a target for blockade in an attempt to selectively prolong atrial APD, thereby preventing or terminating AF. To test this hypothesis both atrial and ventricular nrCMC cultures were treated with 100 nM tertiapin, a specific blocker of $I_{K,ACh}$.¹⁶ Tertiapin significantly increased APD_{80} in atrial nrCMCs during 1-Hz pacing (from 56.5 ± 12.5 to 145.5 ± 20.6 ms, $p < 0.0001$, $n = 33$) (Figure 2B), in the absence of exogenous acetylcholine, showing the presence of $I_{K,ACh-c}$ in these cells (see also Supplemental Results and Supplemental Figure 3). Tertiapin had no significant effect on APD in ventricular nrCMCs ($n = 12$) (Figure 2C). Hence, the increase in APD_{80} induced by tertiapin was significantly larger in atrial nrCMCs (86.7 ± 19.6 vs 9.5 ± 9.9 ms in ventricular nrCMCs) (Figure 2D). Blockade of $I_{K,ACh-c}$ by tertiapin increased APD_{80} during reentry (from 54.7 ± 24.0 to 128.8 ± 16.9 ms, $n = 42$) (Figure 2E-G), which significantly decreased rotor frequency (from 14.1 ± 7.4 to 5.9 ± 1.7 Hz) and complexity (from 6.7 ± 7.7 to 0.58 ± 0.83 PSs) (Figure 2H,I). Interestingly, the inducibility of reentry also decreased (from 89.2 to 27.2%) after tertiapin treatment (Figure 2J). Concomitantly, tertiapin led to complete termination of all rotors in 67.4% of cultures, while rotor termination occurred in only 7.0% of control cultures (Figure 2K).

Figure 1 legend. →

Activation maps (top, 6-ms isochrone spacing) and corresponding phase maps (bottom) of atrial nrCMC cultures during (A) 1-Hz activation showing uniform propagation, (B) three subsequent reentrant cycles after burst pacing showing a stable activation pattern and PS density and localization during each cycle and (C) five subsequent reentrant cycles after burst pacing showing changes in activation pattern and PS density and localization during each cycle. The direction of activation is indicated by the white arrows, PSs are depicted as white circles. Relationship between rotor frequency and (D) APD_{80} , (E) CV and (F) wavelength and between complexity of reentry and (G) APD_{80} , (H) CV and (I) wavelength.

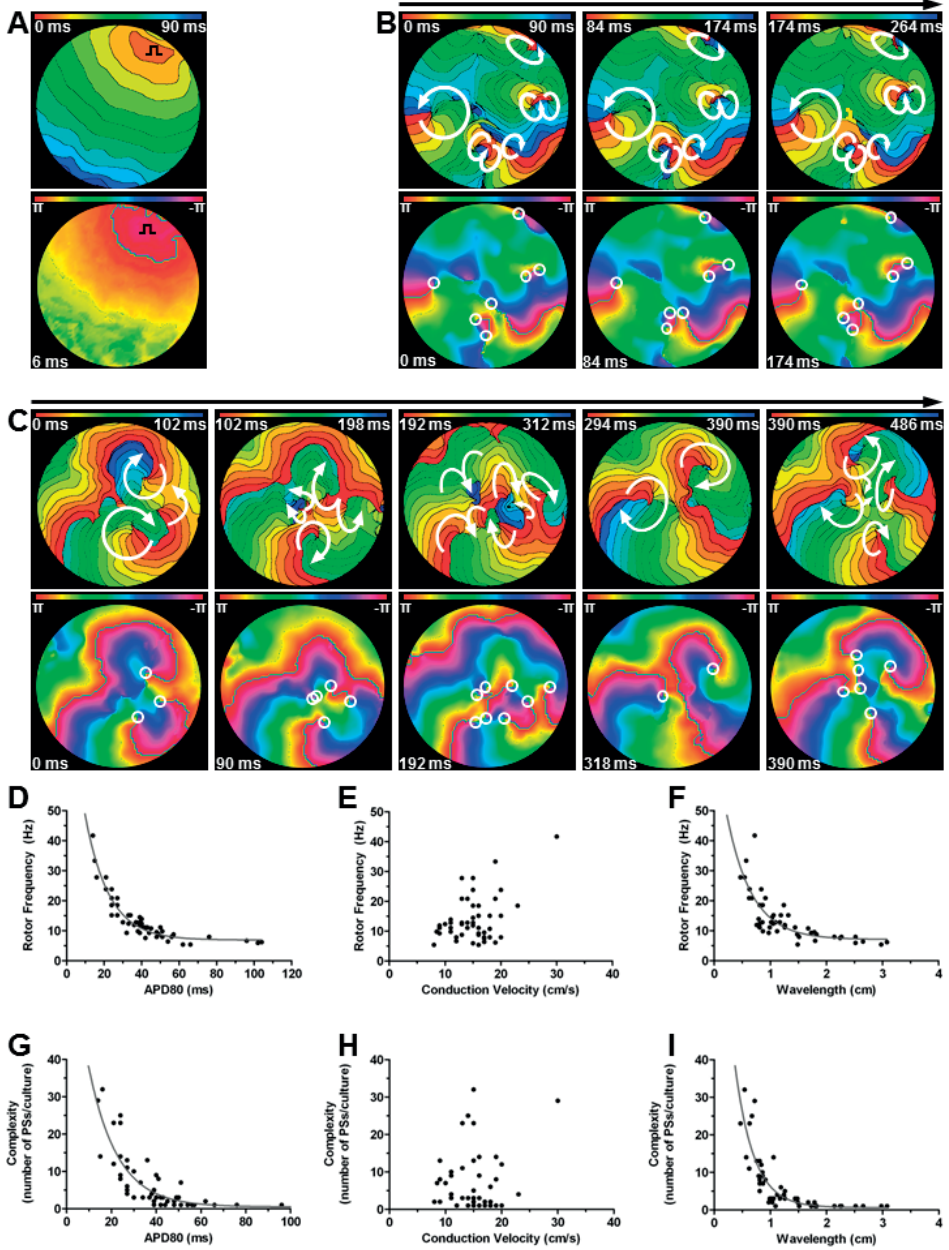
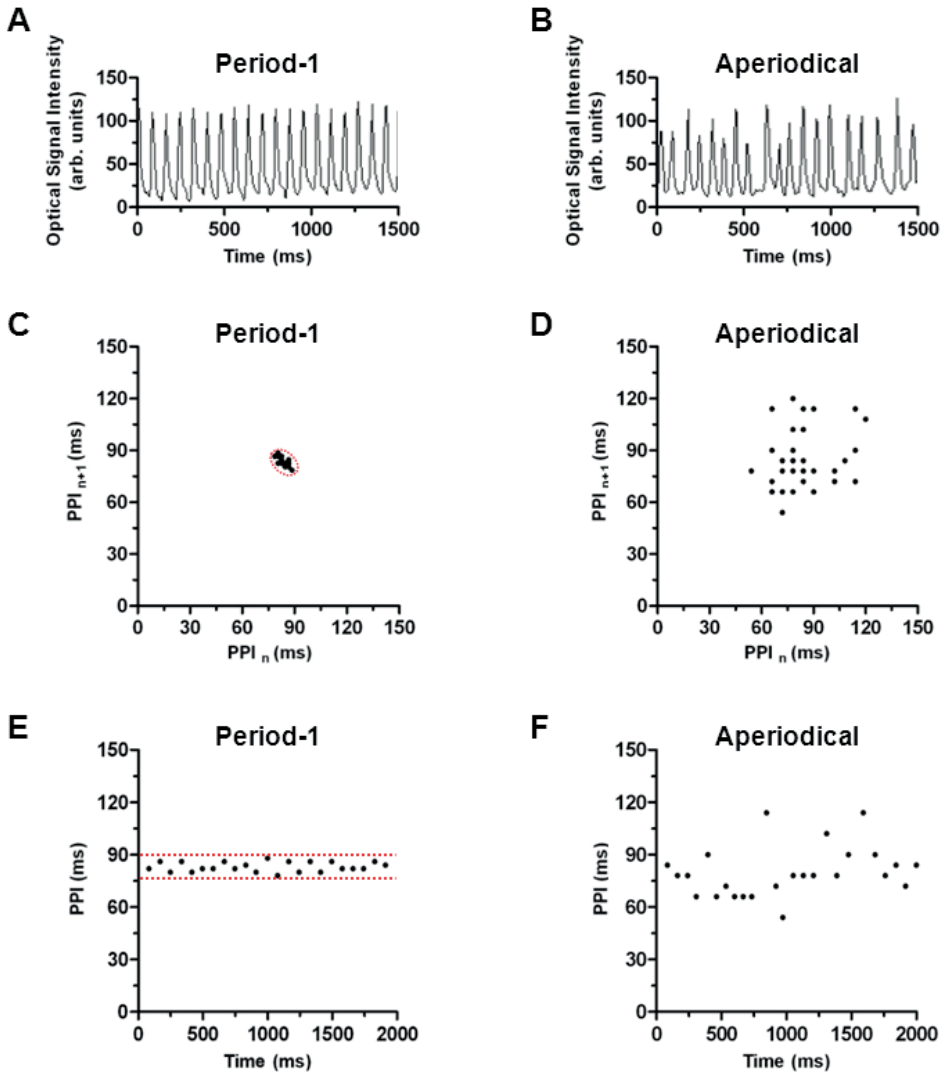


Figure 1



Supplemental Figure II. Typical examples of the optical signal in neonatal rat atrial CMC cultures with (A) period-1 and (B) aperiodical reentry after burst pacing. Return maps of the peak-to-peak interval (PPI) sequences in an atrial CMC culture after burst pacing with (C) period-1 reentry, characterized by monofocal clustering in the return map and (D) aperiodical reentry, characterized by the absence of clustering in the return map. Time series of the PPIs in an atrial CMC culture with (E) period-1 (corresponding with Supplemental Figure II A, C and Figure 1B in the main manuscript) and (F) aperiodical reentry (corresponding with Supplemental Figure II B, D and Figure 1C in the main manuscript). The red dotted lines indicate clustering of PPI sequences and PPIs in the return maps and time series, respectively.

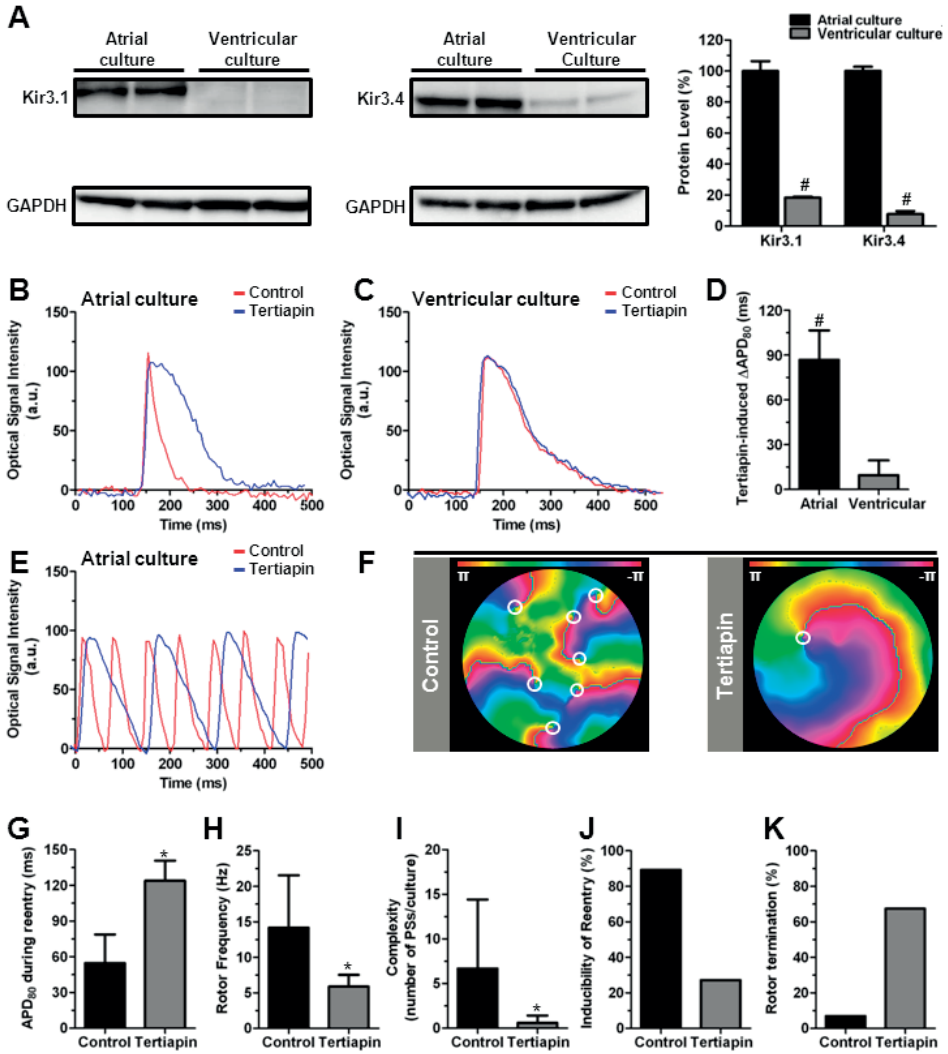


Figure 2 (A) Western blot analysis of Kir3.1 and Kir3.4 levels in atrial and ventricular nCMC cultures using GAPDH as loading control. (B,C) Typical optical AP records of untreated (red) and tertiapin-treated (blue) atrial and ventricular nCMC cultures, respectively. (D) Quantification of ΔAPD_{80} after tertiapin treatment in atrial vs ventricular nCMC cultures. (E) Typical optical signal records of untreated (red) and tertiapin-treated (blue) atrial nCMC cultures after induction of AF by burst pacing. (F) Typical phase maps of untreated (left) and tertiapin-treated (right) cultures after burst pacing. White circles indicate PSs. Quantification of (G) APD_{80} during reentry, (H) rotor frequency, (I) complexity of reentry, (J) inducibility of reentry and (K) complete rotor termination in control and tertiapin-treated atrial nCMC cultures. #: $p < 0.05$ vs atrial cultures, *: $p < 0.05$ vs control, a.u.: arbitrary units.

Kcnj3/5 knockdown in atrial nrCMC cultures

To investigate the individual contribution of the molecular determinants of $I_{K_{ACH-c}}$ (Kir3.1 and Kir3.4) to the induction and dynamics of AF, expression of *Kcnj3* and *Kcnj5* was specifically downregulated in atrial nrCMC cultures by means of lentiviral, shRNA-mediated RNAi. Kir3.1 and Kir3.4 protein levels were significantly lowered in cultures transduced with LV-Kir3.1 \downarrow and LV-Kir3.4 \downarrow , respectively, when compared to those in LV-PpLuc \downarrow -treated control cultures (20.2 ± 1.7 vs 100.0 ± 2.4 and 34.6 ± 3.5 vs $100.0 \pm 34.6\%$, respectively, $n=4$ per group) (Figure 3A-C). As expected, transduction with LV-Kir3.1 \downarrow ($n=11$) and LV-Kir3.4 \downarrow ($n=20$) resulted in significant APD prolongation when compared to PpLuc \downarrow -treated control cultures ($n=11$) (Figure 3D). APD₈₀ was significantly increased throughout all pacing cycle lengths (PCLs) (Figure 3E). Also, CV was lowered significantly by both *Kcnj3* and *Kcnj5* knockdown (Figure 3F), possibly caused by a depolarizing effect of long-term $I_{K_{ACH}}$ downregulation on the resting membrane potential.

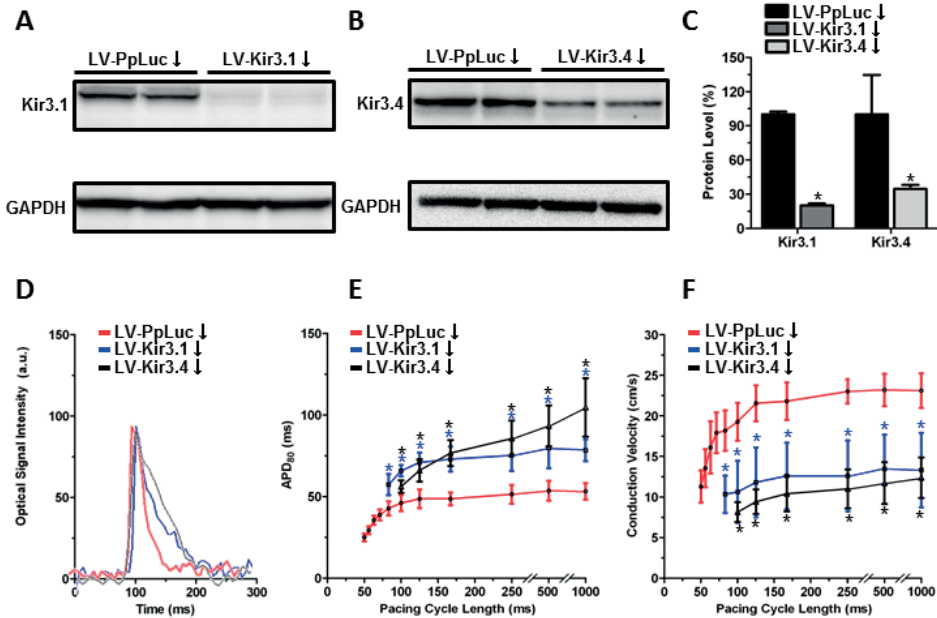


Figure 3. Western blot of (A) Kir3.1 levels in LV-PpLuc \downarrow (i.e. control vector)- and LV-Kir3.1 \downarrow -transduced atrial nrCMC cultures and (B) Kir3.4 levels in LV-PpLuc \downarrow - and LV-Kir3.4 \downarrow -transduced atrial nrCMC cultures using GAPDH as loading control and (C) their quantification. (D) Typical optical signal in atrial nrCMC cultures transduced with the control vector LV-PpLuc \downarrow or with LV-Kir3.1 \downarrow or LV-Kir3.4 \downarrow . Quantification of (E) APD and (F) CV restitution in atrial nrCMC cultures transduced with the control vector LV-PpLuc \downarrow or with LV-Kir3.1 \downarrow or LV-Kir3.4 \downarrow . *: $p < 0.05$ vs LV-PpLuc \downarrow , a.u.: arbitrary units.

Effect of *Kcnj3/5* knockdown on reentry in atrial nrCMC cultures

Next, reentry was induced in cultures transduced with LV-Kir3.1↓(n=14), LV-Kir3.4↓(n=12) or the control LV (n=19) to investigate the effect of Kir3.x-dependent APD prolongation on spiral waves. As expected, reentrant cycle length was significantly increased after knockdown of either *Kcnj3* or *Kcnj5* (Figure 4A-D,F) consistent with prolongation of APD₈₀ during reentry (Figure 4E). Similarly, activation frequency and complexity were significantly decreased (Figure 4G,I, Supplemental Movie 3). In addition, inducibility of reentry was clearly reduced by *Kcnj3* or *Kcnj5* knockdown (Figure 4H). Together, these results show that the effect of tertiapin on reentry induction and dynamics can be reproduced by RNAi-mediated reduction of Kir3.1 or Kir3.4 protein levels.

IK,ACh-c blockade prevents APD alternans by decreasing APD and CV restitution slope

To investigate how $I_{K,ACh-c}$ blockade or downregulation prevents reentry induction we studied the effect of tertiapin on APD and CV restitution. During pacing at 1-20 Hz Kir3.x blockade by tertiapin increased the APD₈₀ throughout all PCLs when compared to control cultures (n=8 per group) (Figure 5A). CV was unaltered following 1-2 Hz pacing after tertiapin treatment. However, at higher pacing frequencies, CV was significantly lower in cultures treated with tertiapin (Figure 5B). This was possibly attributable to a change in the maximal diastolic potential, which gets more depolarized at higher pacing frequencies if the APD is prolonged by $I_{K,ACh-c}$ blockade.²⁰ Furthermore, wavelength was significantly increased by tertiapin at all activation frequencies (Figure 5C). Interestingly, the slope of the APD and CV restitution curves were strongly flattened by tertiapin treatment as a consequence of significantly increased minimal APD₈₀ and decreased maximal activation frequency (Figure 5D,E). As the restitution curves naturally become steeper at shorter diastolic intervals (Figure 5A-C), prolonging minimal APD (and thereby decreasing maximal activation frequency) prevents steepening in APD and also CV restitution. Tertiapin treatment decreased the maximal APD restitution slope from 1.0 ± 0.4 to 0.3 ± 0.2 (Supplemental Figure 4A,B), while the percentage of cultures with a maximal APD restitution slope above the critical value of 1²¹ decreased from 71.4% to 0% (Supplemental Figure 4C).

As a consequence of restitution moderation, spatial (21.7 ± 8.0 vs $56.5 \pm 4.4\%$ in control) and temporal (7.8 ± 6.5 vs $38.1 \pm 8.0\%$ in control) dispersion in APD were significantly decreased by Kir3.x blockade (Figure 5F-I). Since steepening in APD and CV restitution causes small PCL changes to result in large APD and CV changes, APD alternans occurred in control but not in tertiapin-treated cultures. During APD alternans at stable PCL in a control culture, as a consequence of the relationship between APD and diastolic interval (see also Figure 5A) a long APD is repeatedly followed by a short APD, because the diastolic interval is shortened after the long APD (Figure 5G). Because the short APD follows

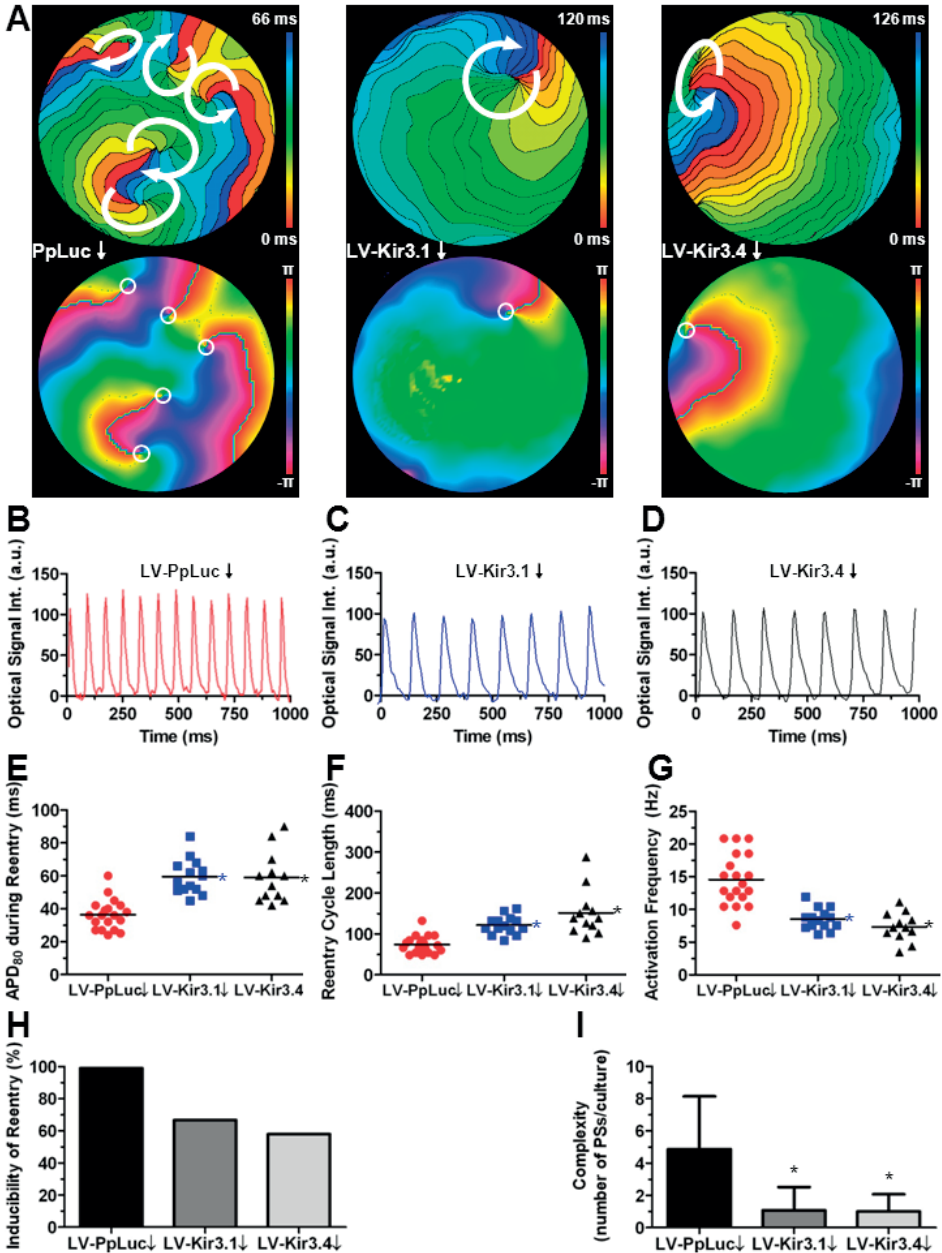


Figure 4. (A) Activation maps and corresponding phase maps during reentry in atrial nrCMC cultures transduced with the control vector LV-PpLuc↓ or with LV-Kir3.1↓ or LV-Kir3.4↓. White arrows indicate the direction of AP propagation, white circles depict PS position. Optical signal traces during reentry in atrial nrCMC cultures transduced with (B) LV-PpLuc↓, (C) LV-Kir3.1↓ or (D) LV-Kir3.4↓. Quantification of (E) APD, (F) cycle length, (G) activation frequency, (H) inducibility of reentry and (I) complexity of reentry after burst pacing in control (red), LV-Kir3.1↓-transduced (blue) and LV-Kir3.4↓-treated (black) atrial nrCMC cultures. *: $p < 0.05$ vs LV-PpLuc↓, a.u.: arbitrary units.

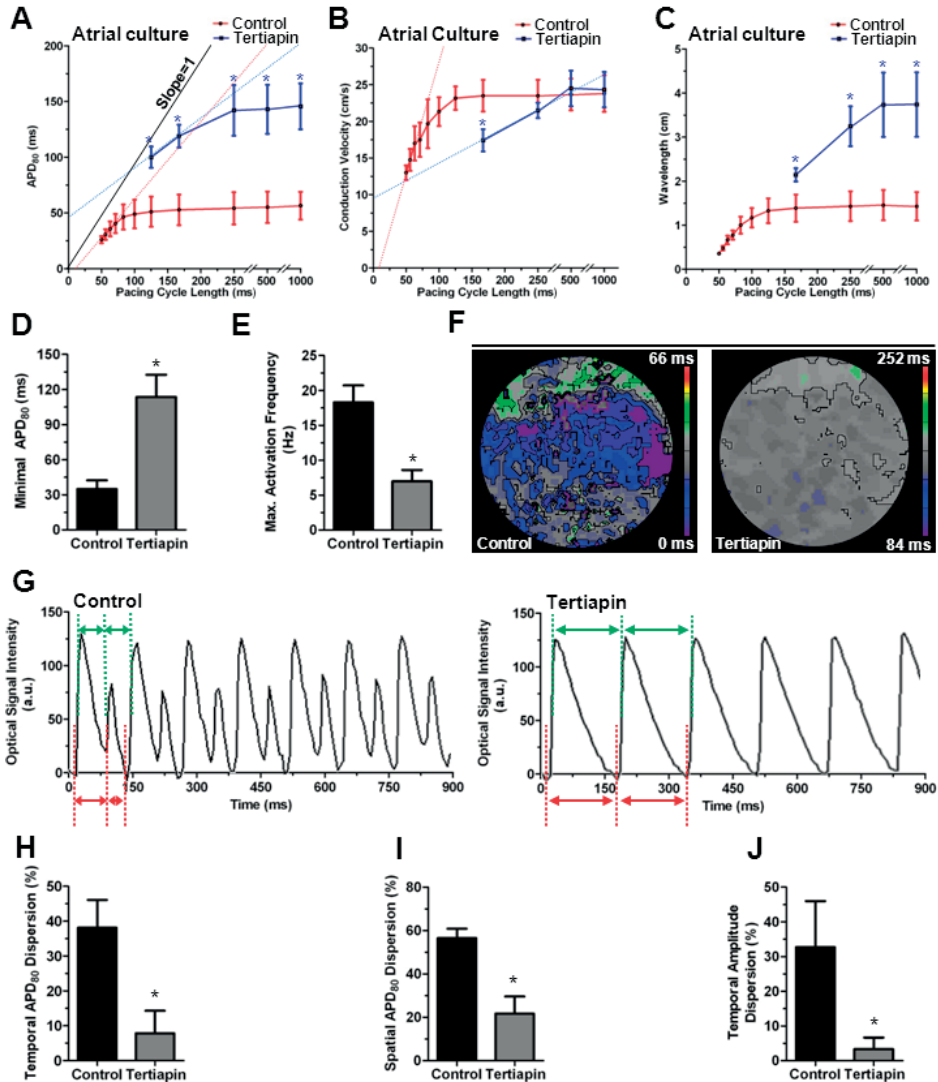
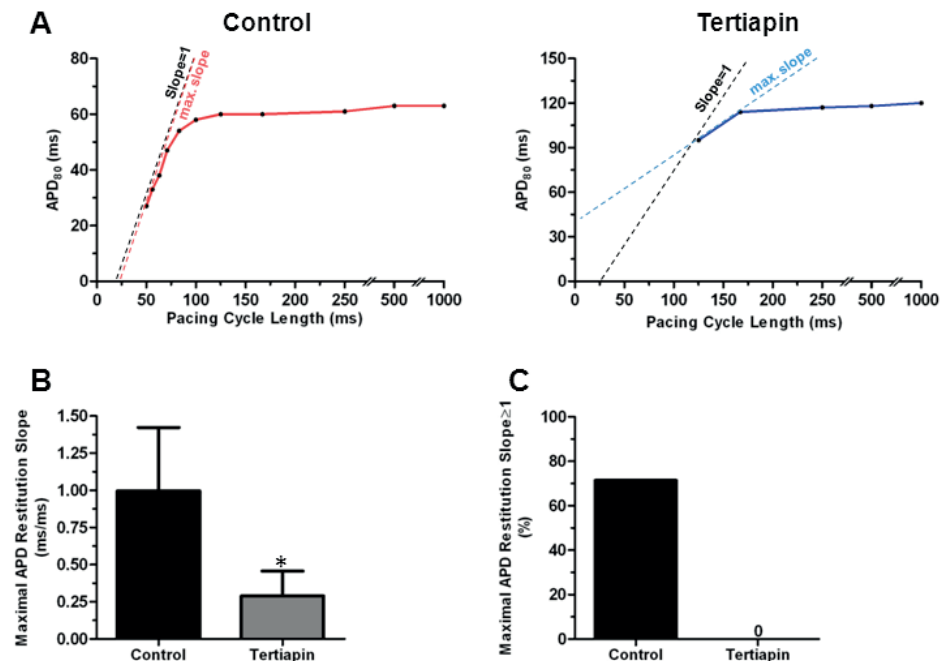


Figure 5. Restitution of (A) APD₈₀, (B) CV and (C) wavelength during 1-20 Hz pacing in control (red) and tertiapin-treated (blue) atrial nCMC cultures. Red and blue dotted lines indicate the maximal slopes in the restitution curves, the solid black line indicates slope=1. Quantification of (D) minimal APD and (E) maximal activation frequency in control and tertiapin-treated atrial nCMC cultures. (F) APD₈₀ maps of untreated (left) and tertiapin-treated (right) atrial nCMC cultures. (G) Typical optical signal traces during pacing at maximal activation frequency in control cultures (left) showing alternating APDs (red double arrows) on equal PCLs (green double arrows) and tertiapin-treated cultures showing stable APDs (red double arrows) on equal PCLs (green double arrows). Quantification of (H) temporal APD₈₀ dispersion, (I) spatial APD₈₀ dispersion and (J) temporal amplitude dispersion. *: $p < 0.05$ vs control, a.u.: arbitrary units.

after incomplete repolarization during the long AP, amplitude alternans occurs (likely due to inactivation of Na^+ channels as a result of incomplete repolarization). Therefore blockade of $I_{\text{K}_{\text{ACh-c}}}$ leads to a significant decrease in temporal amplitude dispersion (Figure 5G,J). Altogether, these findings suggest that $I_{\text{K}_{\text{ACh-c}}}$ -dependent alternans is linked to restitution kinetics (see also Supplemental Results, Supplemental Figure 5).

Role of APD alternans in reentry

In control atrial cultures, reentry initiation after burst pacing was found to be a consequence of highly incident APD alternans, during which a long AP was repeatedly followed by a short AP (Figure 6, left panel). Typically, the long AP was uniformly propagated throughout the culture (Figure 6, right panel, long AP). However, because of the spatial heterogeneity in APD, the short AP frequently underwent conduction block when propagated from an area with short-long APD to an area with long-long APD. This caused PSs to arise adjacent to the area of conduction block (Figure 6, left and right panel, short AP). The AP was subsequently propagated around the PS. This could lead to reentry if the area



Supplemental Figure IV. (A) Typical examples of APD restitution curves of a single control (left) and a single tertiapin-treated (right) culture of neonatal rat atrial CMCs, showing that the maximal slope of the curve in the control culture exceeds 1, while the slope in the tertiapin-treated culture remains well below 1. Black dotted lines indicate slope=1. Colored dotted lines indicate the maximal slope in control (red) and tertiapin-treated (blue) cultures. (B) Quantification of the maximal slope in the APD restitution curve of control and tertiapin-treated cultures. (C) Quantification of the percentage of cultures with a maximal slope in the APD restitution curve ≥ 1 .

in which the conduction block occurred repolarized before return of the wavefront, which then circled the PS in a retrograde fashion (Figure 6, right panel, short AP). These results show that APD alternans, which can be prevented by blockade of $I_{K_{ACh-cr}}$ is a major factor in reentry initiation.

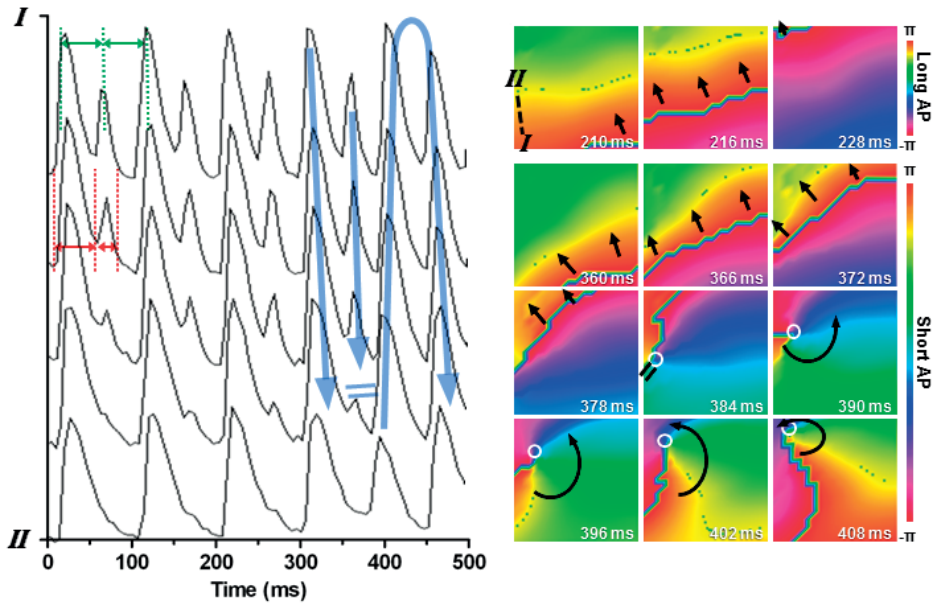


Figure 6. Typical optical signal traces (graph at left side) in a 9-mm² square in a control atrial nrCMC culture during APD alternans leading to reentry. Green and red dotted lines indicate PCL and alternating APD, respectively. Corresponding phase maps (panels at right side) during uniform propagation of the long AP (top panel) and conduction block followed by circular propagation of the short AP (lower panel). Arrows, double lines (blue in the optical signal traces and black in the phase maps) and white circles indicate the direction of AP propagation, conduction block and the PS position, respectively. The positions of points I and II in the culture are indicated in the upper left phase map.

Mechanism of rotor termination after $I_{K_{ACh}}$ blockade

In addition to preventing reentry induction, blockade of $I_{K_{ACh}}$ terminated a large portion of rotors initiated by burst pacing. Atrial cultures were mapped during addition of tertiapin, to study how $I_{K_{ACh}}$ blockade led to rotor termination. Interestingly, during tertiapin incubation rotors with P-1 oscillatory dynamics destabilized into period-2 (P-2) and aperiodical reentry before termination (Figure 7 and Supplemental Figure 6). As shown in Figure 5A, incubation of atrial cultures with tertiapin led to an increase in minimal APD and a decrease in the maximal slope of the APD restitution curve. The higher steepness of the restitution slope at long PCLs in the tertiapin-treated cultures suggests that this slope becomes critically steep before tertiapin has completely increased minimal APD. This caused APD alternans in vulnerable spots during reentry, leading to P-2 oscillatory dynam-

ics (Figure 7, middle panel and Supplemental Figure 6B,D). Subsequently, APD prolonged further and refractory periods around the PSs increased. Consequently, if the refractory period got critically long the reentrant wave had to alter its path from the previous cycle in order to sustain. Therefore, PSs tended to shift position after incubation with tertiapin, leading to aperiodical reentry dynamics (Figure 7, lower panel, Supplemental Figure 6C,D), which simultaneously increased the chance of these PSs to meet a boundary, followed by rotor termination (Figure 7, lower panel, Supplemental Figure 6C,D). As tertiapin increased wavelength and decreased the incidence of APD alternans after full incubation, new rotors are not formed, resulting in a net decrease in complexity of conduction patterns after tertiapin treatment, ultimately leading to termination of AF (Supplemental Movie 4). These results show that apart from affecting reentry initiation and global reentry characteristics, $I_{K_{ACh-c}}$ also determines the period dynamics and propensity towards termination by controlling the onset of APD alternans and PS drift during reentry.

Kir3.x blockade in whole heart mapping

Our novel 2D model of atrial tissue appeared to be crucial for a mechanistic understanding of the role of $I_{K_{ACh-c}}$ in rotor formation, dynamics and termination, as these events are likely to occur subepicardially in the intact atria, which precludes their direct read-out and interpretation. However, whole heart data are needed to show the effects of $I_{K_{ACh-c}}$ on actual AF in a more complex and relevant setting. We thus studied the effects of tertiapin in a whole heart model of AF using neonatal rat hearts. In these hearts, immunocytological analyses confirmed the expression of myosin light chain 2a (MLC2a) in the atria only (Supplemental Figure 7A). The atria consisted of $37.9 \pm 12.1\%$ non-myocytes, which were predominantly fibroblasts as judged by α -actinin/collagen-I double staining (Supplemental Figure 7B,C). Consistent with the *in vitro* results, Western blot analyses showed a significantly higher expression of Kir3.1 and Kir3.4 in the atrium when compared to the ventricle (100.0 ± 21.3 vs $13.7 \pm 6.0\%$ $p < 0.05$ and 100.0 ± 24.2 vs $22.4 \pm 5.2\%$ $p < 0.05$ respectively) (Supplemental Figure 7D). During optical mapping of whole neonatal rat hearts blockade of Kir3.x channels by tertiapin significantly increased atrial APD (62.8 ± 20.9 vs 111.0 ± 32.9 ms, $p < 0.05$) in sinus rhythm while the APD in the ventricles was not significantly altered (219.7 ± 57.6 vs 211.8 ± 42.7 ms, $p < 0.05$) ($n = 10$ per group) (Figure 8A-C). Atropine treatment had no significant effect on atrial APD (54.7 ± 13.9 vs 62.8 ± 20.9 ms in control hearts) (Supplemental Figure 8 A-C), confirming the M2-receptor independent, constitutive activation of $I_{K_{ACh}}$ in neonatal rat atria. After burst pacing, AF was maintained by period-1 oscillatory dynamics in both control and tertiapin-treated hearts. In hearts treated with tertiapin, APD during AF was significantly longer when compared to control hearts (54.8 ± 14.2 ms vs 38.8 ± 7.9 , $p < 0.05$) (Figure 8D,E). As a consequence, AF cycle length was significantly increased (106.5 ± 10.3 vs 81.3 ± 11.3 ms, $p < 0.05$) (Figure 8F), while the inducibility of AF showed a significant decrease after tertiapin incubation

(90% vs 40%, $p < 0.05$) (Figure 8G). Together, these results support the notion that Kir3.x determines the initiation and maintenance of AF in the whole heart.

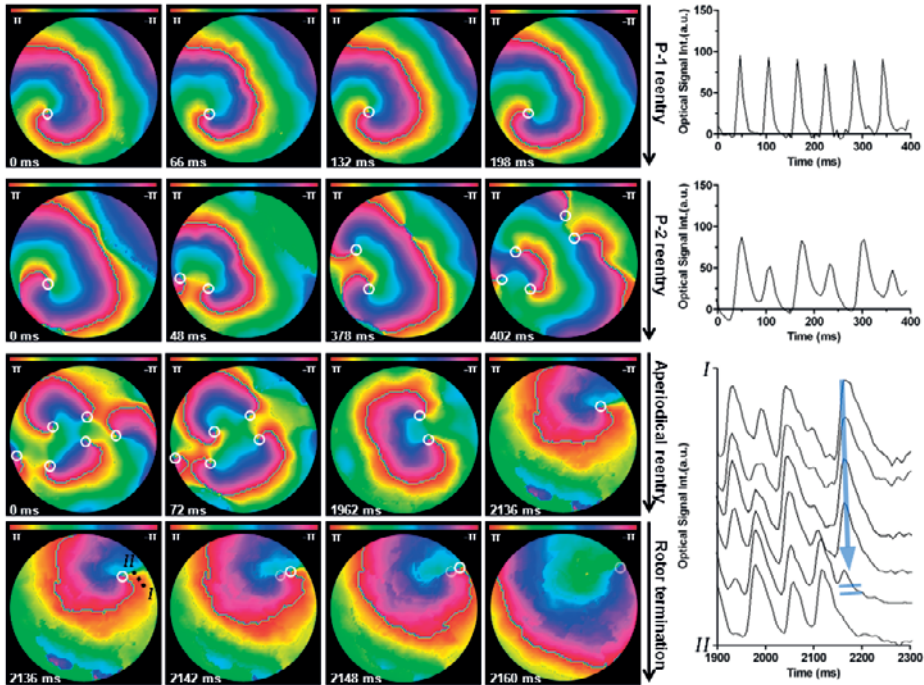
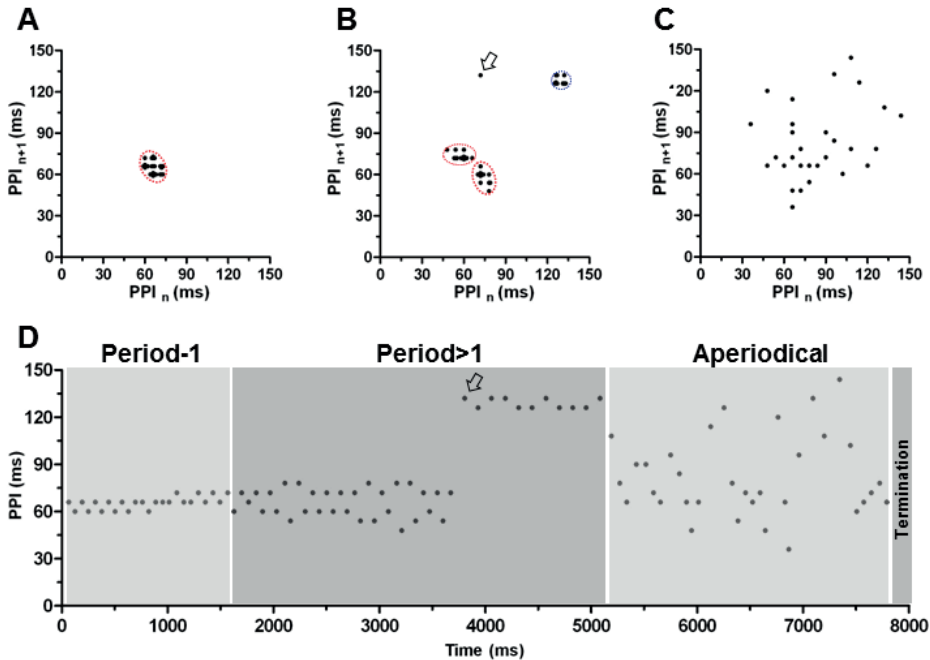


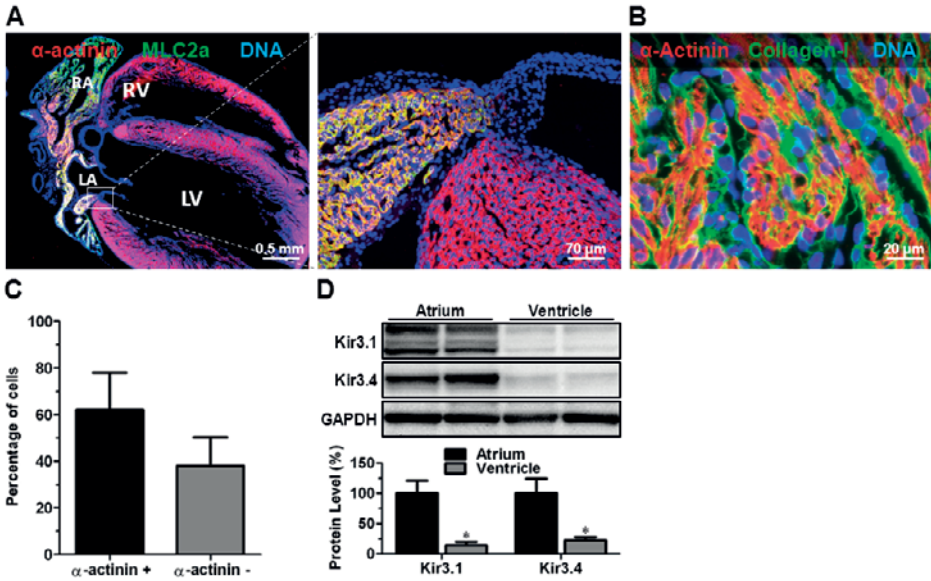
Figure 7. Phase map sequence of an atrial nrCMC culture during tertipin incubation. The upper row shows the initial P-1 reentrant arrhythmia rotating around a single stable PS and its corresponding optical signals. The second row shows the change into a P-2 reentry (approximately 4 s after tertipin addition), with meandering, disappearing and reappearing PSs and its corresponding optical signals showing APD alternans in critical areas. The lower 2 rows show the shift in aperiodical reentry (approximately 9 s after tertipin addition) followed by the termination of rotors as a consequence of PS drift towards the edge of the culture as the wavefront increasingly meets refractory tissue. The white circles indicate PSs, the translucent white circles indicate the PS position in the previous frame. The lower right graph shows the corresponding AP between point I and II in the culture, where the blue arrow indicates the propagation of the final AP leading to conduction block. a.u.: arbitrary units.



Supplemental Figure VI. Return maps of the PPI sequences in an atrial CMC culture during (A) typical period-1 reentry showing a single cluster in the return map, (B) the early phase of tertiapin incubation leading to a change into period-2 reentry showing two clusters (red) as a result of APD alternans (See Figure 7 in the main manuscript, second row) and a third cluster (blue) corresponding to the subsequent prolonged reentrant cycle length (temporary 2:1 conduction) starting at the arrow in both subfigures B and D, (C) the late phase of tertiapin incubation leading to aperiodical reentry lacking any clustering in the return map. Dotted red circles indicate clustering of PPI sequences. (D) Time series of the PPIs during the incubation with tertiapin, showing the progression of period-1, to period>1, to aperiodical reentry and eventually termination. The return maps in A-C are each based on a part of the time series separated by the gray rectangles.

Figure 8 legend. →

(A) Typical examples of a control neonatal rat heart during optical mapping, showing the real image (left panel; left atrium, right atrium ventricles are indicated by the letters LA, RA and V, respectively), a map of atrial activation sequence during sinus rhythm (middle panel, 6-ms isochrone spacing) and a map of the atrial activation sequence during AF induced by burst pacing (right panel, 6-ms isochrone spacing) showing circular activation in the atrial epicardium (white arrow). The white squares indicate the areas from which typical optical signals were derived. (B) Examples of the optical signal traces in the atrium (red) and ventricle (black) in control (left) and tertiapin-treated hearts (right). Quantification of (C) the APD_{80} in atria and ventricles of control and tertiapin-treated hearts during sinus rhythm and (D) of the atrial APD_{80} during AF. (E) Examples of the optical signal traces during AF after burst pacing in the atrium (red) and ventricle (black) in control and tertiapin-treated hearts. Irregularly appearing ventricular traces are indicative of AF. Quantification of (F) AF cycle length and (G) inducibility of AF by burst pacing in control and tertiapin-treated neonatal rat hearts. *: $p < 0.05$ vs control NS: non significant



Supplemental Figure VII. Immunohistological double staining of whole neonatal rat hearts for (A) MLC2a (green) and α -actinin (red) and (B) collagen type I (green) and α -actinin (red). (C) Quantification of the number of α -actinin-positive (i.e. CMCs) and -negative cells (i.e. non-myocytes) as judged by immunohistology. (D) Western blot analysis and quantification of Kir3.1 and Kir3.4 levels in the neonatal rat atrium and ventricle using GAPDH as loading control. LA: left atrium, RA: right atrium, LV: left ventricle, RV: right ventricle, *: $p < 0.05$ vs control.

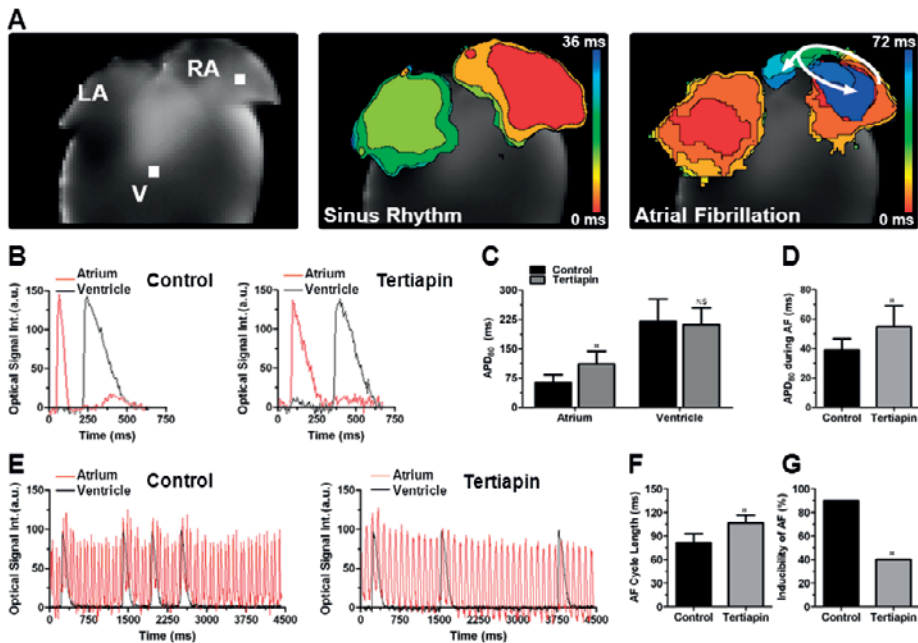
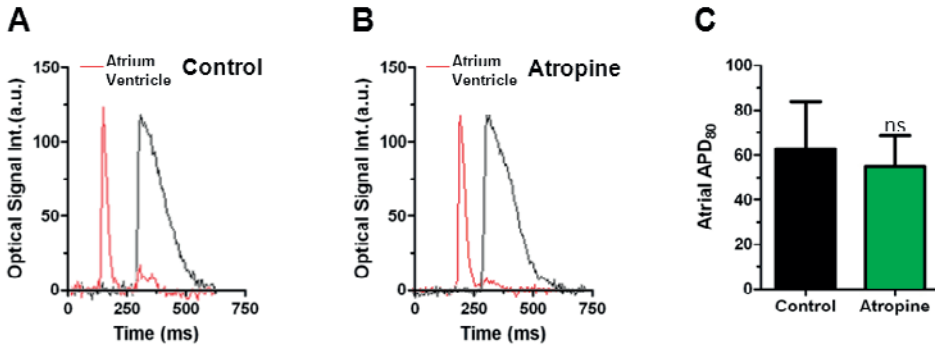


Figure 8.



Supplemental Figure VIII. Typical optical signal traces in the atria (red trace) and ventricles (black trace) of (A) control and (B) atropine-treated neonatal rat hearts. (C) Quantification of APD₈₀ in the atria of control and atropine-treated neonatal rat hearts. NS: non-significant vs control, a.u.: arbitrary units.

DISCUSSION

The key findings of this study are, (1) the acetylcholine-inducible potassium current ($I_{K_{ACh}}$), mediated by Kir3.x, is highly atrium-specific and constitutively active in neonatal rat atrial cell monolayers and intact atria. (2) In the presence of this current, sustained re-entry can be easily induced electrically (~90% incidence), while the incidence decreases strongly after $I_{K_{ACh}}$ blockade. (3) After induction, tachyarrhythmias in atrial cultures are maintained by stable period-1, shifting period >1 or aperiodical rotors, and result from restitution-driven alternans, whereas they are terminated by alternans-mediated PS drift. (4) Mechanistically it is shown by pharmacological and genetic interventions that Kir3.x is a key regulator of these processes of rotor induction, dynamics and termination by controlling APD and APD alternans through APD restitution steepening. (5) Kir3.x represents a promising atrium-specific target for anti-arrhythmic strategies.

Kir3.x in models of AF

Previous studies showed that $I_{K_{ACh}}$ may play an important role in the onset of AF, as acetylcholine activates $I_{K_{ACh}}$ during parasympathetic stimulation and thereby shortens APD.¹⁵ However, after atrial remodeling, which occurs for instance during permanent AF, APD is shortened independently of parasympathetic activation, partly because $I_{K_{ACh}}$ has become constitutively active.¹⁶ While alteration of atrial electrophysiology after atrial remodeling has been established, most of the insights into the electrophysiological mechanisms and complex dynamics of wave propagation in AF have come from detailed investigations in computer and animal models of AF, which did not take into account the molecular consequences of atrial remodeling.²² Hence, these results may be applicable to paroxysmal AF, but translation to persistent AF and AF after atrial remodeling remains difficult. In the current study, models have been used that include one of these molecular consequences, being constitutive activation of $I_{K_{ACh}}$. As such, the present models

might provide a novel means to link the molecular biology of (persistent) AF to its basic electrophysiological mechanisms.²²

We found that the detrimental effects of $I_{K_{ACh-c}}$ are strongly dependent on Kir3.x expression, as is the case when $I_{K_{ACh}}$ is activated by increased parasympathetic tone.^{14,15} As Kir3.1 homomers do not form a functional channel,^{23,24} the preventive effect of *Kcnj3* knockdown is likely attributable to diminished density of Kir3.1/Kir3.4 heteromers at the sarcolemma, while Kir3.4 downregulation affects both Kir3.4 homomers and Kir3.1/Kir3.4 heteromers. This might explain why a 3-fold reduction in Kir3.4 level produced similar results as a 5-fold decrease in Kir3.1 abundance. While earlier studies show that there is very little contribution of Kir3.4 homomers to $I_{K_{ACh}}$,²⁵ our results suggest that after *Kcnj3* knockdown there is still residual $I_{K_{ACh-c}}$, most likely provided by Kir3.4 homomers, the formation of which is inhibited after *Kcnj5* knockdown. This could imply that the contribution of Kir3.x subunits to $I_{K_{ACh}}$ and to its constitutively active counterpart differs.

Nevertheless, the effects of tertiapin on APD, rotor frequency, arrhythmia complexity and inducibility were found to be larger than those of Kir3.1 and Kir3.4 downregulation. As the atrial nrCMCs have a higher tolerability for short-term $I_{K_{ACh-c}}$ blockade by tertiapin as opposed to long-term $I_{K_{ACh-c}}$ blockade by LV-mediated RNAi, tertiapin treatment could provide a somewhat more efficient blockade of $I_{K_{ACh-c}}$ at the moment of electrophysiological analysis. Furthermore, long-term downregulation of Kir3.1 or Kir3.4 seemed to induce a depolarization of the cardiomyocyte membrane potential, decreasing CV even at long PCLs. The conduction-slowing effect of *Kcnj3/5* knockdown by shRNAs strongly diminishes its wavelength-prolonging effect. Therefore, we used tertiapin as an alternative means to study the role of $I_{K_{ACh-c}}$ in AF in whole hearts. The fact that Kir3.1 and Kir3.4 downregulation still strongly decreased inducibility of reentry in atrial cell cultures shows that the effects of $I_{K_{ACh-c}}$ inhibition on the slopes in the restitution curves prevails over its effects on wavelength.

Mechanisms of AF maintenance

For years there has been an ongoing discussion on whether AF is the consequence of single or multiple ectopic focal discharges, the result of reentrant waves or of randomly appearing and disappearing wavelets.²² Isolating the pulmonary veins (PV) can be successful in preventing paroxysmal AF, which could be interpreted as evidence for the focal discharge theory.²⁶ Nevertheless, reentrant sources generating fibrillatory conduction as a consequence of a dominant frequency gradient have been demonstrated in chronic AF.²⁷ Importantly, in patients with a long history of AF, PV isolation has a low success rate.^{5,6} Therefore, at least in permanent AF, reentry seems to play an important role. The presence of a dominant frequency gradient also makes the multiple wavelet hypothesis less plausible, as a hierarchy in frequencies defies randomness as postulated in this theory.²⁸

As demonstrated in our models, constitutive activation of $I_{K,ACH}$ may be one of the determinants of the seemingly increasing role of reentry in the maintenance of AF over time. We show that the constitutively active $I_{K,ACH}$ causes APD alternans, making the atrial tissue prone to wavebreak and reentry initiation. In most cases, after reentry is initiated, multiple stable rotors maintain fibrillation. Without ongoing electrical remodeling, emergence of such rotors in the left atrium would lead to fibrillatory conduction to the right atrium. However, in several cultures we observed AF maintained by shifting aperiodical rotors. As the APD and CV restitution can become critically steep if the $I_{K,ACH}$ is constitutively active, causing both spatial and temporal heterogeneity in repolarization, rotors can meander and break up. Therefore, in the remodeled atrium (*c.q.* with constitutively active $I_{K,ACH}$) random wavelets (*i.e.* random rotors of which the propagated wavefront appear as wavelets at the atrial surface) could maintain AF. This could also explain the possibility of AF originating from a rotor in the right atrium with fibrillatory conduction to the left atrium (for instance after left atrium ablation and permanent AF)²⁸, even though the refractory period is shorter in the left atrium. The fibrillatory aspect of conduction could here be provided by the seemingly random breakup, appearance and disappearance of rotors in the right atrium as opposed to an APD gradient.

APD alternans and AF

Disturbed repolarization is thought to play an important role in producing spatial heterogeneity causing fibrillation in the ventricles. In theory, if fast ectopic firing occurs, for instance from the PVs, spatial heterogeneity in repolarization would also favor reentry initiation in the atria. Hence, it has recently been proposed that repolarization alternans could also play an important role in AF. Indeed, it has been shown that atrial repolarization alternans occurs frequently before initiation of AF.²⁹⁻³¹ In the diseased atrium changes in calcium handling have been shown to cause the APD to alternate as a consequence of calcium instabilities.³² During calcium-dependent APD alternans, APD restitution is not necessarily altered. We show here for the first time that APD alternans underlying reentry can be caused by constitutive activation of $I_{K,ACH}$ which steepens APD restitution. Hence, we confirm that disturbed atrial repolarization is associated with the onset of AF. In addition to this association we show experimentally that wavebreak and resultant reentry are the direct consequence of APD alternans. Earlier *in silico* work predicted that discordant APD alternans leads to wavebreak if the short AP in a long-short sequence reaches the refractory tail of a long AP in a short-long sequence. In accordance with these predictions, we found that propagation of a short AP of an alternating long-short sequence halts when it meets the refractory tail of a long AP. However, in our model the long AP was usually not the consequence of discordant APD alternans, *e.g.* a short-long sequence. Instead, it was the result of a large APD dispersion causing areas with APD alternans to border areas with solely long APDs. Thus, in our model, we provide

an extension to the aforementioned theory by showing that spatial APD dispersion in combination with APD alternans (while not being classically discordant) can cause AF in cells with constitutively active $I_{K,ACh}$.

Atrial fibrosis in AF

Atrial fibrosis is thought to be an important component of AF substrates.³³ In this study, atrial cell cultures consisted of approximately 17% cardiac fibroblasts as deduced by collagen type I immunostaining. Previous studies showed that atrial conduction abnormalities as a consequence of fibrosis strongly depend on the pattern of fibrosis.³⁴ It was found that long fibrotic strands of tissue could cause significant conduction abnormalities, and thereby contribute to AF, while diffuse fibrosis only marginally affected conduction. In our *in vitro* model, fibroblasts are diffusely spread. Also, the percentage of fibroblasts in this model is lower than in intact neonatal rat atria (see also Supplemental figures 1F and 7B,C). In spite of this difference in fibroblast content the atrial cell culture and whole heart models yielded very similar results in terms of the inducibility of AF and the ability to suppress AF by $I_{K,ACh-c}$ blockade. Furthermore, in both our *in vitro* and whole heart model, pathological conditions that promote fibrosis are absent. It thus appears that in our models a possible contribution of fibroblast to AF induction is overshadowed by the strong pro-arrhythmic effects of $I_{K,ACh-c}$.

Study limitations

The present study made use of nrCMCs and neonatal rat hearts, which differ electrophysiologically from the more clinically relevant adult human cardiomyocytes and hearts. Use of cardiomyocytes from human adults is hampered by the difficulties to (i) obtain human cardiac tissue of sufficient quality for the isolation of cardiomyocytes and (ii) maintain human cardiomyocytes in a differentiated state during culture. In addition, healthy atrial nrCMCs were used to facilitate the study of Kir3.x and $I_{K,ACh-c}$. It should be noted, however, that constitutive activation of $I_{K,ACh}$ in human atrial myocytes is usually preceded by significant atrial remodeling and hence may have a different origin than in our model. Hence, our study focused on a proof-of principle, investigating the role of $I_{K,ACh}$ on APD alternans, AF prevention and termination irrespective of its onset. As such, the results may not be directly extrapolatable to the clinical setting.

CONCLUSIONS

In neonatal rat atrial cell monolayers and intact atria, the acetylcholine-inducible potassium current is constitutively active and plays a crucial role in the initiation of sustained tachyarrhythmias. Mechanistically it is shown in atrial cell monolayers that $I_{K,ACh-c}$ is

mediated by Kir3.x and not only regulates the initiation but also the maintenance and termination of these arrhythmias by controlling APD and APD alternans through APD restitution steepening. Accordingly, this study provides insights into the molecular basis of atrium-specific $I_{K_{ACH-c}}$ and revealed the crucial role it could play in pro- and anti-arrhythmic mechanisms in atrial tissue. These novel insights could contribute to the development of mechanistically driven and atrium-specific, anti-arrhythmic strategies.

FUNDING

This work was supported by the Dutch Heart Foundation (E. Dekker grant [2012/T023 to B.O.B.]) and the Netherlands Organisation for Scientific Research (NWO; VENI grant [91611070 to D.A.P.]).

ACKNOWLEDGEMENTS

We wish to thank Huybert J.F. van der Stadt for excellent technical support.

CONFLICT OF INTEREST DISCLOSURES

None.

SUPPLEMENTAL MATERIAL

METHODS

All animal experiments were approved by the Animal Experiments Committee of the Leiden University Medical Center and conformed to the Guide for the Care and Use of Laboratory Animals as stated by the US National Institutes of Health.

Cell isolation and culture

Ventricular and atrial cardiomyocytes (CMCs) were isolated from 2-3 old neonatal Wistar rats by collagenase digestion as described previously.³⁵ Isoflurane inhalation (4-5%) was used to anaesthetize animals. After adequate anesthesia had been confirmed by the absence of pain reflexes, hearts were excised. Subsequently, large vessels were removed and atria were separated from ventricles. Atrial and ventricular tissue was gently minced and digested using collagenase type 1 (450 U/ml; Worthington, Lakewood, NJ) and DNase I (18,75 Kunitz/ml; Sigma-Aldrich, St. Louis, MO) during 2 subsequent 30-min digestion steps with agitation in a water bath at 37°C. Cell suspensions were pre-plated on Primaria-coated culture dishes (Becton Dickinson, Breda, the Netherlands) for 120 min to allow for preferential attachment of non-myocytes. Next, the unattached cells (mainly CMCs) were passed through a nylon cell strainer with a mesh pore size of 70 μm (Becton Dickinson) to remove cell aggregates and, after counting, the cells were plated isotropically on fibronectin (Sigma-Aldrich)-coated, round glass coverslips (15-mm diameter) in 24-well plates (Corning Life Sciences, Amsterdam, the Netherlands). Cell densities of $2\text{-}8 \times 10^5$ cells/well were used depending on the experiment. To restrict unwanted expansion of the remaining non-myocytes, cell proliferation was inhibited by incubation with Mitomycin-C (10 $\mu\text{g}/\text{ml}$; Sigma-Aldrich) for 2 h at day 1 of culture as described previously.^{35,36} All cultures were refreshed daily with Dulbecco's modified Eagle's medium (DMEM)/HAM's F10 (1:1, v/v; both from Life Technologies, Bleiswijk, the Netherlands) supplemented with 5% horse serum (Life Technologies) and cultured in a humidified incubator at 37°C and 5% CO_2 .

Immunocytology

Cells were stained for the markers of interest after several rinses with ice-cold phosphate-buffered saline (PBS) to wash out the culture medium, fixation with 1% formaldehyde in PBS and permeabilization with 0.1% Triton X-100 in PBS. Primary antibodies (1:200 dilution in PBS+5% fetal bovine serum [FBS; Life Technologies]) and corresponding Alexa Fluor 488/568-conjugated secondary antibodies (1:400 dilution in PBS+5% FBS; Life Technologies) were left on the cells for 16 and 2 h, respectively, at 4°C. Cultures were stained using antibodies directed against α -actinin (Sigma-Aldrich) as CMC marker,

myosin light chain 2a (MLC2a; a gift from Dr. S.W. Kubalak, Charleston, SC) and natriuretic peptide precursor A (NPPA, Merck Millipore, Billerica, MA) as markers for atrial CMCs and myosin light chain 2v (MLC2v; Synaptic Systems, Goettingen, Germany) to identify ventricular CMCs. Non-myocytes were characterized immunostaining using antibodies specific for collagen type I (fibroblasts; Abcam, Cambridge, MA), platelet endothelial cell adhesion molecule-1 (PECAM-1; endothelial cells; Abcam) and smooth muscle myosin heavy chain (smMHC; smooth muscle cells; Abcam). Primary antibodies specific for connexin40 (Cx40; Santa Cruz Biotechnology, Dallas, TX) and connexin43 (Cx43; Sigma-Aldrich) were used to determine expression of gap junction proteins. Counterstaining of the nuclei was performed by a 5-min incubation at room temperature with 10 µg/ml Hoechst 33342 (Life Technologies) in PBS+5% FBS. Cells were rinsed twice with PBS+5% FBS after incubation with primary antibodies, secondary antibodies and Hoechst 33342. Coverslips were mounted in Vectashield mounting medium (Vector Laboratories, Burlingame, CA) to minimize photobleaching. Images were taken at equal exposure times between compared groups using a fluorescence microscope equipped with a digital color camera (Nikon Eclipse 80i; Nikon Instruments Europe, Amstelveen, the Netherlands). Dedicated software (NIS Elements [Nikon Instruments Europe] and ImageJ [version 1.43; National Institutes of Health, Bethesda, MD]) were used to store and quantify immunofluorescence signals, respectively. All proteins of interest were studied in at least 3 different cultures per experimental group, from which at least 15 representative images were taken.

Immunohistology

Neonatal rat hearts were rinsed with PBS, fixed overnight using 4% formaldehyde in PBS and dehydrated by immersion in 70% ethanol (3 h), 96% ethanol (3 h), 100% ethanol (3 h) and 1-butanol (overnight), respectively. Hearts were embedded in paraffin, cut in 5-µm-thick sections and mounted on StarFrost adhesive microscope slides (Knittel Glass, Braunschweig, Germany). Next, sections were deparaffinized in xylene and rehydrated by the subsequent immersion in 100% ethanol, 96% ethanol, 70% ethanol and PBS for 5 min each. Antigen retrieval was performed by incubating the slides with 0.05% trypsin and 0.1% CaCl₂ in demineralized water at pH 7.8 for 15 min at 37°C and 15 min at 20°C, respectively. Sections were immunostained overnight with the aforementioned primary antibodies directed against MLC2a, α-actinin and collagen type I diluted 1:100 in PBS with 1% bovine serum albumin (BSA; Sigma-Aldrich) and 1% Tween-20 (PBSBT). Corresponding secondary antibodies (Alexa Fluor 488/568-conjugated antibodies, Life Technologies) diluted in PBSBT were incubated for 2 hours, after which the nuclei were counterstained with 10 µg/ml Hoechst 33342 in PBSBT. Image acquisition, processing and analysis were done using the fluorescence microscope and software described above.

Western blotting

CMC cultures were rinsed twice with ice-cold PBS to wash out the culture medium. Next, the cells were lysed in RIPA buffer (50 mM Tris-HCl [pH 8.0], 150 mM NaCl, 1% Triton X-100, 0.5% sodium deoxycholate, 0.1% sodium dodecyl sulfate supplemented with protease inhibitors [cOmplete, Mini Protease Inhibitor Cocktail Tablet; Roche Applied Science, Penzberg, Germany]). Lysates were subsequently flash frozen in liquid nitrogen, thawed and centrifuged at 4°C and 21,130×g for 15 min to get rid of undissolved material. The protein concentration in the supernatant was determined using BCA Protein Assay Reagent (Thermo Fisher Scientific, Etten-Leur, the Netherlands). Proteins (10 µg per sample; ≥3 samples per group) were then size-fractionated in NuPage Novex 12% Bis-Tris gels (Life Technologies) and transferred to Hybond polyvinylidene difluoride membranes (GE Healthcare, Diegem, Belgium) by wet electroblotting. Membranes were blocked in Tris-based saline, 0.1% Tween-20 (TBST) supplemented with 5% BSA for 1 h at room temperature. Next, the blots were incubated with primary antibodies directed against Cx40 (1:1,000), Cx43 (1:100,000), Kir3.1 (1:1,000; Alomone Labs, Jerusalem, Israel), Kir3.4 (1:1,000; Santa Cruz Biotechnology), MLC2a (1:200,000), MLC2v (1:5,000), NPPA (1:5,000) and glyceraldehyde 3-phosphate dehydrogenase (1:120,000; loading control; Merck Millipore) for 1 h at room temperature in TBST+5% BSA. Following 3 rinses with TBST, the blots were incubated with appropriate horseradish peroxidase-conjugated secondary antibodies (Santa Cruz Biotechnology) diluted 1:1,000 in TBST+5% BSA for 1 h at room temperature. After another 3 rinses with TBST, membranes were immersed in ECL Prime Western blot detection reagent (GE Healthcare) and chemiluminescence was captured using the ChemiDoc XRS imaging system (Bio-Rad Laboratories, Veenendaal, the Netherlands).

For Western blotting of whole hearts, hearts were excised, atria and ventricles were carefully separated and rinsed in ice-cold PBS before lysis in RIPA buffer using a TissueLyser LT (QIAGEN, Benelux, Venlo, the Netherlands). The whole heart lysates were subsequently processed in the same manner as the lysates of cultured cells.

Construction of self-inactivating lentivirus (SIN-LV) shuttle plasmids

To repress rat *Kcnj3* expression, a SIN-LV shuttle construct encoding a short hairpin (sh) RNA targeting mouse *Kcnj3*, and matching perfectly with the coding sequence of the rat *Kcnj3* gene, was obtained from the MISSION shRNA library (Sigma-Aldrich; clone TRCN0000069736). To knock down rat *Kcnj5* expression, the hybridization product of oligodeoxyribonucleotides 5' CCGGGACCACAAGAAGATCCCCAAACTCGAGTTTGGGGATCTTCTTGTGGTCTTTTTG 3' and 5' AATTCAAAAAGACCACAAGAA-GATCCCCAAACTCGAGTTTGGGGATCTTCTTGTGGTC 3' was inserted in between the unique SgrAI and EcoRI recognition sites of SHC007 (MISSION shRNA library; Sigma-Aldrich) to replace its *Photinus pyralis luciferase (PpLuc)*-specific shRNA-coding sequence. Next, the marker gene cassette in these constructs and in SHC007, which

consisted of the human *phosphoglycerate kinase 1* gene promoter and the puromycin-N-acetyltransferase-coding sequence was replaced by the human *eukaryotic translation elongation factor 1 alpha 1* gene promoter and the *Aequorea victoria* enhanced green fluorescent protein (eGFP)-coding sequence. This yielded the SIN-LV shuttle plasmids pLKO.1-mKcnj3-shRNA.hEEF1a1.eGFP, pLKO.1-rKcnj5-shRNA.hEEF1a1.eGFP and pLKO.1-PpLuc-shRNA.hEEF1a1.eGFP, which were used to generate LV-Kir3.1↓, LV-Kir3.4↓ and LV-PpLuc↓ particles, respectively.

SIN-LV production

Vesicular stomatitis virus G protein-pseudotyped SIN-LV particles were generated by transfecting subconfluent monolayers of 293T cells with the packaging plasmids psPAX2 (Addgene, Cambridge, MA; plasmid number: 12260) and pLP/VSVG (Life Technologies) and one of the 3 aforementioned SIN-LV shuttle constructs at a molar ratio of 2:1:1. The 293T cells were cultured in high-glucose DMEM containing 10% FBS. The transfection mixture, which consisted of 40 µg of plasmid DNA and 120 µg of polyethyleneimine (Polysciences Europe, Eppelheim, Germany) in 2 ml of 150 mM NaCl per 175-cm² cell culture flask (Greiner Bio-One, Alphen aan den Rijn, the Netherlands) was directly added to the culture medium. Sixteen hours later, the transfection medium in each flask was replaced by 15 ml of DMEM supplemented with 5% FBS and 25 mM HEPES-NaOH (pH 7.4). At 40-48 h after the start of the transfection procedure, the culture medium was harvested and cleared from cellular debris by centrifugation for 10 min at 3,000×g and filtration through a 33-mm diameter, 0.45-µm pore size polyethersulfone syringe filter (Millex Express; Merck Millipore). To concentrate and purify the SIN-LV particles, 30 ml of vector suspension were layered onto a 5-ml cushion of 20% (wt/vol) sucrose in PBS and centrifuged at 15,000 rotations per min for 2 h at 4°C in an SW32 rotor (Beckman Coulter, Fullerton, CA). Next, the supernatant was discarded and the pellet containing the SIN-LV particles was suspended in 500 µl of PBS-1% BSA by gentle rocking overnight at 4°C. The concentrated vector suspension was divided in 50-100 µl aliquots and stored at -80°C until use. The 3 SIN-LVs were applied to the atrial CMC cultures at doses that resulted in transduction of essentially all cells in the cultures. The transduction level was assessed using a Zeiss Axiovert 200M inverse fluorescence microscopy to visualize eGFP fluorescence.

In vitro optical mapping

At day 9 of culture, action potential (AP) propagation was investigated on a whole-culture scale by optical mapping using the voltage-sensitive dye di-4-ANEPPS (Life Technologies) as described previously.^{35,36} During optical mapping cells were stimulated electrically using a custom-made, epoxy-coated unipolar platinum electrode with square suprathreshold electrical stimuli at 1 and 2-20 Hz (2-Hz increments). Fibrillation was induced by burst pacing with a cycle length of 20-100 ms. A specialized electri-

cal stimulus module with corresponding software (Multichannel Systems, Reutlingen, Germany) was used to perform electrical stimulation. Data analysis and construction of activation maps were performed with specialized software (BrainVision Analyzer 1101; Brainvision, Tokyo, Japan) after pixel signals were averaged with 8 of its nearest neighbors, to minimize noise artifacts. Conduction velocity (CV) in cultures with uniform or reentrant activation patterns was calculated perpendicular to the activation wavefront, between two 3 by 3 pixel grids typically spaced 2-8 mm apart. CV, activation frequency, APD during maximal paced activation frequency (*i.e.* minimal APD) and APD during 1 Hz pacing were determined at 6 different locations equally distributed throughout the culture and averaged before further analysis. APD was determined at 80% of repolarization (APD₈₀) because of the rat AP shape. Wavelength was calculated by multiplying average CV with APD₈₀ (for uniform propagation) or reentrant cycle length.³⁵ Complexity was defined as the number of phase singularities (PSs) per culture, determined by using the phase space method as described previously.³⁵ The effect of several drugs (100 nmol/L tertiapin [Alomone Labs], 200 nmol/L atropine (Sigma-Aldrich) and 2 μmol/L carbachol (Sigma-Aldrich)¹⁶ was studied by pipetting them directly into the medium, dispersing them by gentle agitation, immediately followed by optical mapping.

Whole heart mapping

Neonatal (2-3 days old) Wistar rats were anesthetized by isoflurane inhalation (4-5%) and adequate anesthesia was confirmed by the absence of pain reflexes. Subsequently, the thoracic wall was cut and lifted to expose the heart. Oxygenated Tyrode's solution (comprising [in mM] NaCl 130, CaCl₂ 1.8, KCl 4.0, MgCl₂ 1.0, NaH₂PO₄ 1.2, NaHCO₃ 24 and glucose 5.5 at pH 7.4) supplemented with 20 mM 2,3-butanedione monoxime (Sigma-Aldrich, BDM) with or without 200 nM tertiapin to minimize motion artifacts and to block Kir3.x channels, respectively, was carefully injected in a 200 μL bolus into the left ventricle using a 30-G needle. The heart was excised just prior to absence of visible contractions, and submersed in Tyrode's solution with BDM and tertiapin to remove remaining blood. Next, hearts were incubated in Tyrode's solution with BDM and tertiapin containing 2 μM di-4-ANEPPS for 2 min at 37°C, after which the heart was rinsed and submersed in Tyrode's solution with BDM and tertiapin and placed on top of a 37°C heating plate under the optical mapping camera. AF was induced by burst pacing at a cycle length of 20-100 ms using a custom-made bipolar platinum electrode. Control hearts were treated in an identical manner except that tertiapin was left out during the entire procedure. Typical optical mapping experiments were performed within 6 min after excision of the heart.

RESULTS

Cell culture characterization

Immunocytological analysis at day 9 of culture showed that 100% of the CMCs (*i.e.* α -actinin-positive cells) in the atrial cell cultures were MLC2a-positive (*i.e.* of atrial origin) while in the ventricular cell cultures no MLC2a-positive CMCs were detected (Supplemental Figure IA,C). In addition, NPPA levels were much higher in the atrial than in the ventricular CMC cultures (Supplemental Figure IB). Western blot analyses confirmed these results and showed that MLC2v was exclusively present in the ventricular cell cultures. (Supplemental Figure ID). Atrial CMC cultures contained more Cx40 than the ventricular CMC cultures, while Cx43 levels were higher in ventricular CMCs as judged by both Western blotting (Supplemental Figure ID) and immunocytology (Supplemental Figure IE). Atrial cell cultures were also analyzed by collagen type I, PECAM-1 and smMHC staining. While none of the cells contained detectable amounts of PECAM-1 or smMHC, $17.0 \pm 2.5\%$ of the cells stained positive for collagen-I (Supplemental Figure IF) suggesting that the non-myocytes in atrial cell cultures consisted mainly, if not exclusively, of fibroblasts.

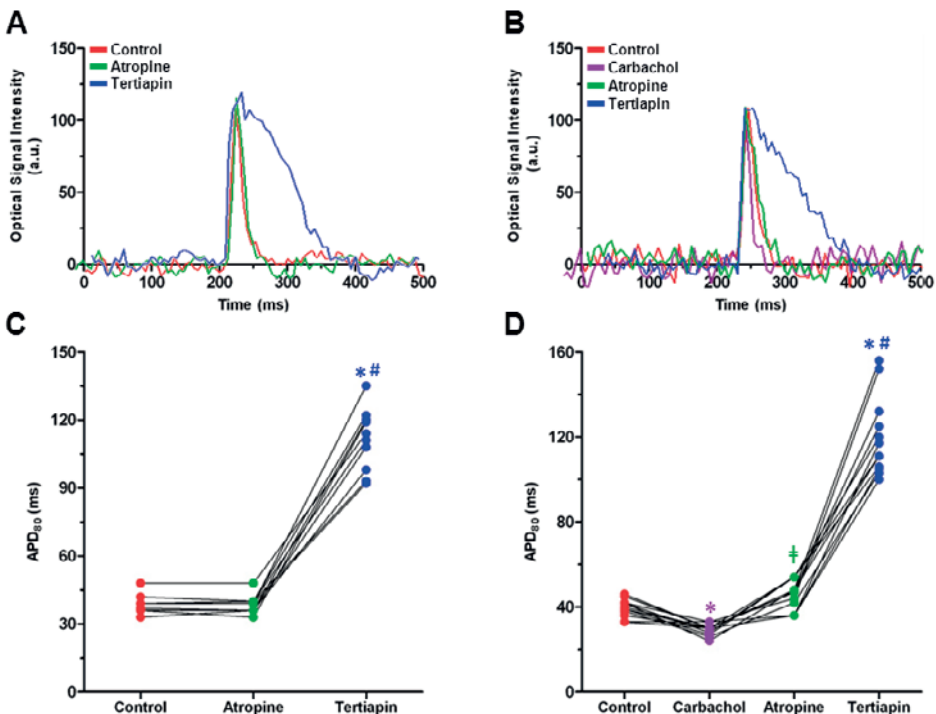
Constitutive activation of I_{KACH} in neonatal rat atrial CMC cultures

During constitutive activation I_{KACH} becomes activated independently of acetylcholine or the acetylcholine receptor. Therefore, to confirm constitutive I_{KACH} (I_{KACH-c}) activity in our neonatal rat atrial CMC cultures, atropine (a non-selective muscarinic receptor antagonist) was used to block the acetylcholine receptor during optical mapping to study the dependence of APD on acetylcholine receptor activation. Atropine had no significant effect on the APD_{80} (38.5 ± 3.9 vs 38.6 ± 3.9 ms in control cultures, $p=ns$), whereas subsequent treatment with tertiapin significantly increased APD_{80} (to 110.9 ± 13.1 ms, $p < 0.0001$) (Supplemental Figure IIIA,C). This illustrates that after blockade of the acetylcholine receptor there is still current flowing through Kir3.x channels shortening APD. Thus, our cultures of neonatal rat atrial CMCs indeed possess I_{KACH-c} activity. Nonetheless, treatment of neonatal rat atrial CMCs with carbachol (a non-selective muscarinic receptor agonist) induced a significant shortening of APD_{80} (from 39.6 ± 4.2 to 29.3 ± 3.9 ms, $p < 0.0001$). After subsequent atropine treatment APD_{80} rose to 45.6 ± 6.9 ms, ($p < 0.0001$ vs carbachol-treated cells) abolishing the carbachol-induced APD shortening, while addition of tertiapin to the carbachol- and atropine-treated CMCs again greatly increased APD_{80} (to 119.8 ± 18.5 , $p < 0.0001$ vs [carbachol- and] atropine-treated cells) (Supplemental Figure IIIB,D). Together, these results show that the short AP in neonatal rat atrial CMC cultures is caused by a tertiapin-sensitive current which is independent of ligand-induced muscarinic receptor activation and therefore constitutively active. The cells, however, also still possess muscarinic receptor stimulation-dependent Kir3.x activity given the APD shortening-effect of carbachol treatment and its inhibition by atropine.

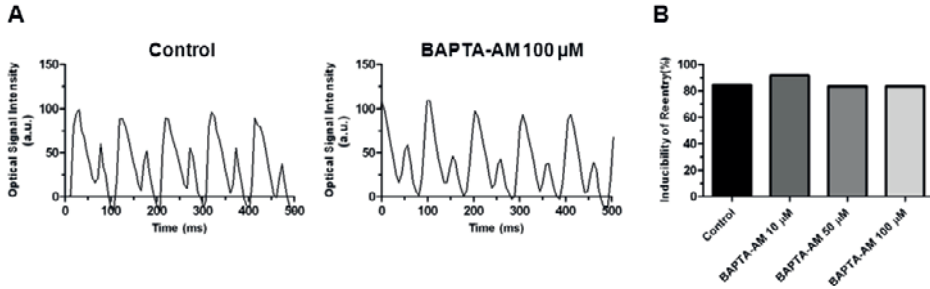
APD alternans in neonatal rat atrial CMCs is independent of intracellular $[Ca^{2+}]$

To confirm the restitution-based nature of APD alternans, neonatal rat atrial CMC cultures were treated with the cell-permeable Ca^{2+} chelator BAPTA-AM (10-100 $\mu\text{mol/L}$; Life Technologies) to rule out the contribution of intracellular Ca^{2+} to APD alternans and reentry induction. Successful buffering of intracellular Ca^{2+} was confirmed by phase contrast microscopy, showing absence of visible contractions after incubation with 10 $\mu\text{mol/L}$ BAPTA-AM during 1-Hz pacing (data not shown).

Treatment with BAPTA-AM did not prevent APD alternans (Supplemental Figure VA), while the frequency of reentry induction after burst pacing remained equal for all tested concentrations of BAPTA-AM (84.6% in controls vs 91.7%, 83.3% and 83.3% after treatment of the cells with 10, 50 or 100 $\mu\text{mol/L}$ BAPTA-AM, respectively) (Supplemental Figure VB). This suggests that APD alternans and consequential reentry induction in our model are driven by the $I_{K_{\text{ACh-c}}}$ -induced steepness in the APD/CV restitution curve.



Supplemental Figure III. (A) Typical examples of optical signal traces in a neonatal rat atrial CMC culture before (control) and after the cumulative treatment with 200 nmol/L atropine and 100 nmol/L tertiapin during 1-Hz pacing. (B) Typical examples of optical signal traces in a neonatal rat atrial CMC culture before (control) and after the cumulative treatment with 2 $\mu\text{mol/L}$ carbachol, 200 nmol/L atropine and 100 nmol/L tertiapin during 1-Hz pacing. (C) Quantification of APD₈₀ at a 1-Hz pacing frequency in untreated atrial CMC cultures and in atrial CMC cultures treated with atropine and tertiapin, respectively. (D) Quantification of APD₈₀ at a 1-Hz pacing frequency in untreated atrial CMC cultures and in atrial CMC cultures treated with carbachol, atropine and tertiapin, respectively. *: $p < 0.05$ vs control, #: $p < 0.05$ vs atropine, ‡: $p < 0.05$ vs carbachol.



Supplemental Figure V. (A) Typical examples of optical signal traces of control (left) and BAPTA-AM-treated (right) neonatal rat atrial CMC cultures at maximal activation frequency in areas showing APD alternans (B) Quantification of reentry inducibility in control cultures and in cultures treated with 10 $\mu\text{mol/L}$, 50 $\mu\text{mol/L}$ or 100 $\mu\text{mol/L}$ BAPTA-AM showing no difference in the induction of reentry by burst pacing during buffering of intracellular Ca^{2+} .

Movie 1: Typical example from an optical mapping experiment in a neonatal rat atrial CMC culture after burst pacing showing period-1 reentry dynamics. The first part shows the high-pass-filtered optical signal exemplifying the repeating activation pattern during period-1 reentry. The second part displays the phase map progression of the same optical mapping experiment, showing the wave propagation around multiple PSs with fixed positioning throughout the experiment.

Movie 2: Typical example from an optical mapping experiment in a neonatal rat atrial CMC culture after burst pacing showing aperiodical reentry dynamics. The first part shows the high-pass-filtered optical signal exemplifying the transient activation pattern during aperiodical reentry. The second part displays the phase map progression of the same optical mapping experiment, showing multiple instances of PS formation and disappearance leading to aperiodical dynamics.

Movie 3: Typical example from an optical mapping experiment in neonatal rat atrial cultures investigating the effect of treatment with LV-Kir3.1 \downarrow , LV-Kir3.4 \downarrow or the control vector LV-PpLuc \downarrow after reentry induction by burst pacing. The high-pass-filtered optical signal shows less complex conduction patterns and a lower activation frequency in cell cultures that had been transduced with the Kcnj3- or Kcnj5-specific shRNA-coding SIN-LV than in those exposed to the control vector.

Movie 4: Typical movie from optical mapping experiment investigating the effect of tertiapin on reentry dynamics and termination. Part 1 shows the high-pass-filtered optical signal in an atrial culture after burst pacing during the first 500 ms after tertiapin incubation, which is characterized by persisting rotors and period-1 dynamics. The second part shows the high-pass-filtered optical signal in an atrial culture after a few seconds of tertiapin incubation, characterized by drifting rotors and aperiodical dynamics, which is followed by termination (part 3) when the last rotor collides with the culture boundary.

REFERENCE LIST

1. Lloyd-Jones DM, Wang TJ, Leip EP, Larson MG, Levy D, Vasan RS, D'Agostino RB, Massaro JM, Beiser A, Wolf PA, Benjamin EJ. Lifetime risk for development of atrial fibrillation: the Framingham Heart Study. *Circulation*. 2004;110:1042-1046.
2. Miyasaka Y, Barnes ME, Bailey KR, Cha SS, Gersh BJ, Seward JB, Tsang TS. Mortality trends in patients diagnosed with first atrial fibrillation: a 21-year community-based study. *J Am Coll Cardiol*. 2007;49:986-992.
3. Wolowacz SE, Samuel M, Brennan VK, Jasso-Mosqueda JG, Van Gelder IC. The cost of illness of atrial fibrillation: a systematic review of the recent literature. *Europace*. 2011;13:1375-1385.
4. Calkins H, Kuck KH, Cappato R, Brugada J, Camm AJ, Chen SA, Crijns HJ, Damiano RJ, Jr., Davies DW, DiMarco J, Edgerton J, Ellenbogen K, Ezekowitz MD, Haines DE, Haissaguerre M, Hindricks G, Iesaka Y, Jackman W, Jalife J, Jais P, Kalman J, Keane D, Kim YH, Kirchhof P, Klein G, Kottkamp H, Kumagai K, Lindsay BD, Mansour M, Marchlinski FE, McCarthy PM, Mont JL, Morady F, Nademanee K, Nakagawa H, Natale A, Nattel S, Packer DL, Pappone C, Prystowsky E, Raviele A, Reddy V, Ruskin JN, Shemin RJ, Tsao HM, Wilber D. 2012 HRS/EHRA/ECAS Expert Consensus Statement on Catheter and Surgical Ablation of Atrial Fibrillation: recommendations for patient selection, procedural techniques, patient management and follow-up, definitions, endpoints, and research trial design. *Europace*. 2012;14:528-606.
5. Oral H, Knight BP, Tada H, Ozaydin M, Chugh A, Hassan S, Scharf C, Lai SW, Greenstein R, Pelosi F, Jr., Strickberger SA, Morady F. Pulmonary vein isolation for paroxysmal and persistent atrial fibrillation. *Circulation*. 2002;105:1077-1081.
6. Brooks AG, Stiles MK, Laborderie J, Lau DH, Kuklik P, Shipp NJ, Hsu LF, Sanders P. Outcomes of long-standing persistent atrial fibrillation ablation: a systematic review. *Heart Rhythm*. 2010;7:835-846.
7. Cappato R, Calkins H, Chen SA, Davies W, Iesaka Y, Kalman J, Kim YH, Klein G, Packer D, Skanes A. Worldwide survey on the methods, efficacy, and safety of catheter ablation for human atrial fibrillation. *Circulation*. 2005;111:1100-1105.
8. Weerasooriya R, Khairy P, Litalien J, Macle L, Hocini M, Sacher F, Lellouche N, Knecht S, Wright M, Nault I, Miyazaki S, Scavee C, Clementy J, Haissaguerre M, Jais P. Catheter ablation for atrial fibrillation: are results maintained at 5 years of follow-up? *J Am Coll Cardiol*. 2011;57:160-166.
9. Coplen SE, Antman EM, Berlin JA, Hewitt P, Chalmers TC. Efficacy and safety of quinidine therapy for maintenance of sinus rhythm after cardioversion. A meta-analysis of randomized control trials. *Circulation*. 1990;82:1106-1116.
10. Echt DS, Liebson PR, Mitchell LB, Peters RW, Obias-Manno D, Barker AH, Arensberg D, Baker A, Friedman L, Greene HL, . Mortality and morbidity in patients receiving encainide, flecainide, or placebo. The Cardiac Arrhythmia Suppression Trial. *N Engl J Med*. 1991;324:781-788.
11. Ehrlich JR and Nattel S. Novel approaches for pharmacological management of atrial fibrillation. *Drugs*. 2009;69:757-774.
12. Hohnloser SH and Singh BN. Proarrhythmia with class III antiarrhythmic drugs: definition, electrophysiologic mechanisms, incidence, predisposing factors, and clinical implications. *J Cardiovasc Electrophysiol*. 1995;6:920-936.
13. Waldo AL, Camm AJ, deRuyter H, Friedman PL, MacNeil DJ, Pauls JF, Pitt B, Pratt CM, Schwartz PJ, Veltri EP. Effect of d-sotalol on mortality in patients with left ventricular dysfunction after recent and remote myocardial infarction. The SWORD

- Investigators. Survival With Oral d-Sotalol. *Lancet*. 1996;348:7-12.
14. Dobrzynski H, Marples DD, Musa H, Yamashita TT, Henderson Z, Takagishi Y, Honjo H, Kodama I, Boyett MR. Distribution of the muscarinic K⁺ channel proteins Kir3.1 and Kir3.4 in the ventricle, atrium, and sinoatrial node of heart. *J Histochem Cytochem*. 2001;49:1221-1234.
 15. Liu L and Nattel S. Differing sympathetic and vagal effects on atrial fibrillation in dogs: role of refractoriness heterogeneity. *Am J Physiol*. 1997;273:H805-H816.
 16. Dobrev D, Friedrich A, Voigt N, Jost N, Wettwer E, Christ T, Knaut M, Ravens U. The G protein-gated potassium current I(K,ACh) is constitutively active in patients with chronic atrial fibrillation. *Circulation*. 2005;112:3697-3706.
 17. Ehrlich JR, Cha TJ, Zhang L, Chartier D, Villeneuve L, Hebert TE, Nattel S. Characterization of a hyperpolarization-activated time-dependent potassium current in canine cardiomyocytes from pulmonary vein myocardial sleeves and left atrium. *J Physiol*. 2004;557:583-597.
 18. Bingen BO, Askar SF, Schalij MJ, Kazbanov IV, Ypey DL, Panfilov AV, Pijnappels DA. Prolongation of Minimal Action Potential Duration in Sustained Fibrillation Decreases Complexity by Transient Destabilization. *Cardiovasc Res*. 2012;97:161-170
 19. Askar SF, Ramkisoensing AA, Schalij MJ, Bingen BO, Swildens J, van der Laarse A, Atsma DE, de Vries AA, Ypey DL, Pijnappels DA. Antiproliferative treatment of myofibroblasts prevents arrhythmias in vitro by limiting myofibroblast-induced depolarization. *Cardiovasc Res*. 2011;90:295-304.
 20. Kleber AG and Rudy Y. Basic mechanisms of cardiac impulse propagation and associated arrhythmias. *Physiol Rev*. 2004;84:431-488.
 21. Nolasco JB and Dahlen RW. A graphic method for the study of alternation in cardiac action potentials. *J Appl Physiol*. 1968;25:191-196.
 22. Jalife J. Deja vu in the theories of atrial fibrillation dynamics. *Cardiovasc Res*. 2011;89:766-775.
 23. Hedin KE, Lim NF, Clapham DE. Cloning of a *Xenopus laevis* inwardly rectifying K⁺ channel subunit that permits GIRK1 expression of IKACH currents in oocytes. *Neuron*. 1996;16:423-429.
 24. Krapivinsky G, Gordon EA, Wickman K, Velimirovic B, Krapivinsky L, Clapham DE. The G-protein-gated atrial K⁺ channel IKACH is a heteromultimer of two inwardly rectifying K(+) channel proteins. *Nature*. 1995;374:135-141.
 25. Bettahi I, Marker CL, Roman MI, Wickman K. Contribution of the Kir3.1 subunit to the muscarinic-gated atrial potassium channel IKACH. *J Biol Chem*. 2002;277:48282-48288.
 26. Medi C, Sparks PB, Morton JB, Kistler PM, Halloran K, Rosso R, Vohra JK, Kumar S, Kalman JM. Pulmonary vein antral isolation for paroxysmal atrial fibrillation: results from long-term follow-up. *J Cardiovasc Electrophysiol*. 2011;22:137-141.
 27. Kalifa J, Jalife J, Zaitsev AV, Bagwe S, Warren M, Moreno J, Berenfeld O, Nattel S. Intra-atrial pressure increases rate and organization of waves emanating from the superior pulmonary veins during atrial fibrillation. *Circulation*. 2003;108:668-671.
 28. Hocini M, Nault I, Wright M, Veenhuyzen G, Narayan SM, Jais P, Lim KT, Knecht S, Matsuo S, Forclaz A, Miyazaki S, Jadidi A, O'Neill MD, Sacher F, Clementy J, Hais-saguerre M. Disparate evolution of right and left atrial rate during ablation of long-lasting persistent atrial fibrillation. *J Am Coll Cardiol*. 2010;55:1007-1016.
 29. Narayan SM, Bode F, Karasik PL, Franz MR. Alternans of atrial action potentials during atrial flutter as a precursor to atrial fibrillation. *Circulation*. 2002;106:1968-1973.
 30. Gong Y, Xie F, Stein KM, Garfinkel A, Cuianu CA, Lerman BB, Christini DJ.

- Mechanism underlying initiation of paroxysmal atrial flutter/atrial fibrillation by ectopic foci: a simulation study. *Circulation*. 2007;115:2094-2102.
31. Hiromoto K, Shimizu H, Furukawa Y, Kanemori T, Mine T, Masuyama T, Ohyanagi M. Discordant repolarization alternans-induced atrial fibrillation is suppressed by verapamil. *Circ J*. 2005;69:1368-1373.
 32. Tsai CT, Chiang FT, Tseng CD, Yu CC, Wang YC, Lai LP, Hwang JJ, Lin JL. Mechanical stretch of atrial myocyte monolayer decreases sarcoplasmic reticulum calcium adenosine triphosphatase expression and increases susceptibility to repolarization alternans. *J Am Coll Cardiol*. 2011;58:2106-2115.
 33. Schotten U, Verheule S, Kirchhof P, Goette A. Pathophysiological mechanisms of atrial fibrillation: a translational appraisal. *Physiol Rev*. 2011;91:265-325.
 34. Kawara T, Derksen R, de Groot JR, Coronel R, Tasseron S, Linnenbank AC, Hauer RN, Kirkels H, Janse MJ, de Bakker JM. Activation delay after premature stimulation in chronically diseased human myocardium relates to the architecture of interstitial fibrosis. *Circulation*. 2001;104:3069-3075.
 35. Bingen BO, Askar SF, Schalij MJ, Kazbanov IV, Ypey DL, Panfilov AV, Pijnappels DA. Prolongation of minimal action potential duration in sustained fibrillation decreases complexity by transient destabilization. *Cardiovasc Res*. 2013;97:161-170.
 36. Askar SF, Ramkisoensing AA, Schalij MJ, Bingen BO, Swildens J, van der Laarse A, Atsma DE, de Vries AA, Ypey DL, Pijnappels DA. Antiproliferative treatment of myofibroblasts prevents arrhythmias in vitro by limiting myofibroblast-induced depolarization. *Cardiovasc Res*. 2011;90:295-304.

